BM@N Analysis Note 2
Production of Λ hyperons in 4.0 and 4.5 A GeV carbon-nucleus interactions

Analysis team: M.Kapishin, G.Pokatashkin,
I.Rufanov, Yu.Stepanenko, V.Vasendina, A.Zinchenko

Abstract

Production of Λ hyperons in interactions of the carbon beam with the kinetic energy 4.0 and 4.5 AGeV with the *C, Al, Cu, Pb* targets was studied with the BM@M detector at the Nuclotron. The analysis procedure is described in details. Results on Λ hyperon yields have been obtained and compared with model predictions and data available.

BM@N configuration in the carbon beam run

The technical run of the BM@N detector was performed with the carbon beam in March 2017. The view of the BM@N setup used in the run is presented in Fig. 1 (left). The configuration of the central tracker was based on one plane of a forward silicon detector and six GEM stations combined from 5 GEM detectors with the size of 66x41 cm^2 and 2 GEM detectors with the size of 163x45 cm^2 [GEMTDR]. The tracking stations were arranged to have the beam passing through their centers (Fig. 1 (right)). Each successive GEM station was rotated by 180^o around the vertical axis. It was done to have the opposite electron drift direction in the successive stations in order to avoid a systematic shift of reconstructed tracks due to the Lorentz angle in the magnetic field. The research program was devoted to measurements of inelastic reactions $C+A \rightarrow X$ with the beam kinetic energy of 4.0 and 4.5A GeV and different targets: *C, Al, Cu, Pb*. The technical program of the run included the measurement of the carbon beam momentum in the central and outer tracker at different values of the magnetic field. Since the GEM tracker configuration was tuned to measure relatively high-momentum beam particles, the geometric acceptance for relatively soft decay products of strange *V0* particles was rather low.

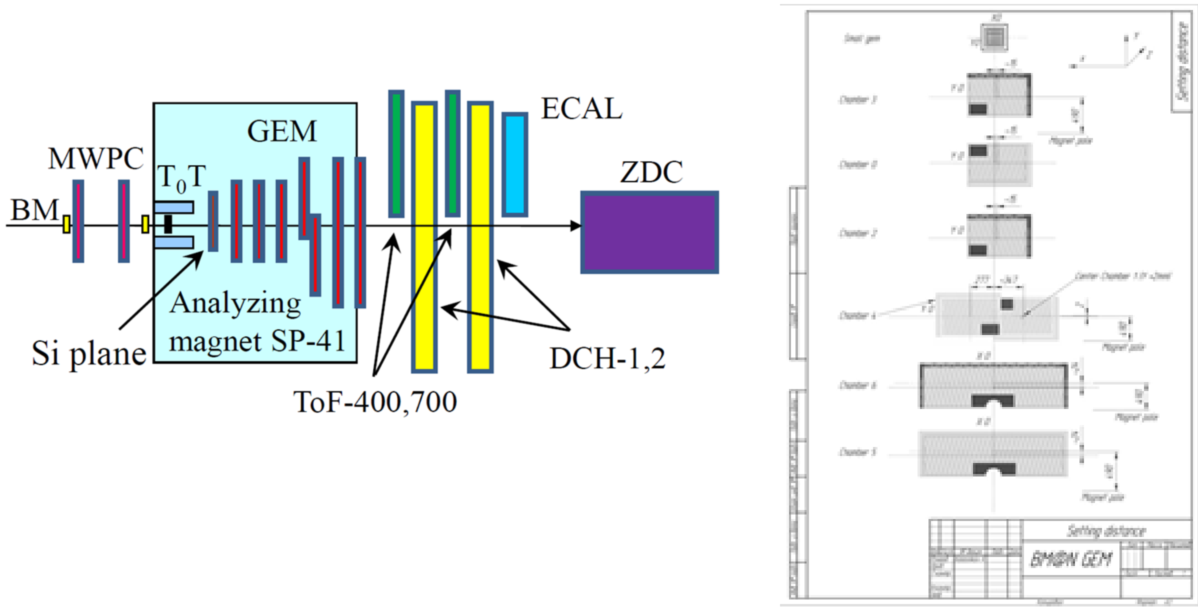

Fig. 1. Left plot: BM@N set-up in the carbon beam run. Right plot: configuration of the GEM detectors, see a more detailed plot at [GEMconf].

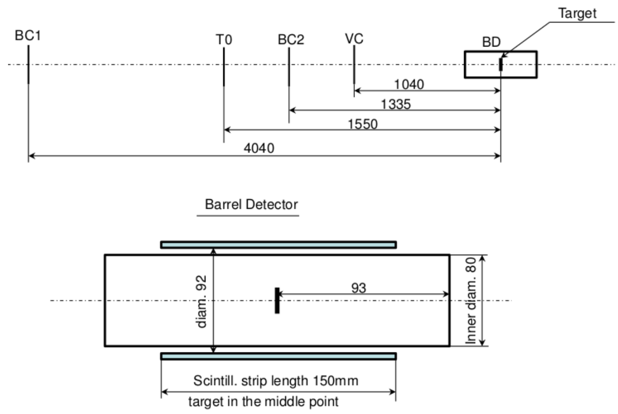

Fig.1b. Schematic view and positions of the beam counters, barrel detector and target.

In the present analysis the experimental data from the forward silicon detector, GEM detectors, trigger barrel multiplicity detector, beam, veto and T0 counters were used. The positions of the beam counters and trigger barrel detector and the target are given in Fig.1b. The carbon beam intensity was few 10^5 per the spill, the spill duration was 2-2.5 sec. The magnetic field in the center of the analyzing magnet was 0.61 T.

Monte Carlo simulation and event reconstruction

The Monte Carlo event samples of *C+A* collisions were produced with the DCM-QGSM event generator. The passage of particles through the setup volume was simulated with the GEANT program integrated into the BmnRoot software framework. To properly describe the GEM detector response in the magnetic field the microsimulation package Garfield++ was used. The package gives very detailed description of the processes inside the GEM detector, including the drift and diffusion of released electrons in electric and magnetic fields and the electron multiplication in GEM foils, so that the output signal from the readout plane can be reproduced. To speed up the simulation, dependencies of the Lorentz shifts and the charge distributions on the readout planes on the drift distance were parameterized and used in the GEM digitization part of the BmnRoot package. The details of the detector alignment, Lorenz shift corrections are described in the paper [DeuteronPaper]. The track reconstruction method was based on the so-called “cellular automaton" approach [CBM1]. The tracks found were used to reconstruct primary and secondary vertices using the “KF-particle" formalism [CBM2]. Λ hyperons were reconstructed using their decay mode into two oppositely-charged tracks. The signal event topology (decay of a relatively long-lived particle into two tracks) defined the selection criteria: small track-to-track separation in the decay vertex, relatively large decay length of the mother particle. Since particle identification was not used in the analysis, all positive tracks were considered as protons and all negative as π^-.

Event selection criteria:

1. Number of tracks in selected events: positive>=1, negative>=1;
2. Beam halo, pile-up suppression within the readout time window: number of signals in the start detector: T0=1, number of signals in the beam counter: BC2=1, number of signals in the veto counter around the beam: Veto=0;
3. Trigger condition in the barrel detector: number of signals BD>=2 or BD>=3 (run dependent).

The suppression factors of reconstructed events ε_{pileup} due to selection criteria 2 applied to eliminate beam halo and pile-up events in interactions of the 4.0 and 4.5 AGeV carbon beam with the *C, Al, Cu, Pb* targets are given in Table 1.

Table 1. ε_{pileup} suppression factors.

Selection	4 AGeV	4.5 AGeV
T0==1	+	+
BC2==1	+	+
Veto==0	+	+
C	0.674	0.529
Al	0.740	0.618
Cu	0.779	0.621
Pb	0.784	0.686

The total suppression factors are applied to reduce the recorded beam fluxes and luminosities which are summarized in Table 2.

Table 2. Number of triggered events, beam fluxes and integrated luminosities collected in interactions of the carbon beam of 4.0 and 4.5AGeV with different targets.

Interactions, target thickness	Number of triggers / 10^6	Integrated beam flux / 10^7	Integrated luminosity / 10^{30} cm^{-2}
4 AGeV, *C*+*C* (9 mm)	3.98	6.07	6.06
4 AGeV, *C*+*Al* (12 mm)	3.81	3.31	2.39
4 AGeV, *C*+*Cu* (5 mm)	4.77	4.71	2.00
4 AGeV, *C*+*Pb* (10 mm)	0.67	0.67	0.22

Interactions, target thickness	Number of triggers / 10^6	Integrated beam flux / 10^7	Integrated luminosity / 10^{30} cm^{-2}
4.5 AGeV, *C*+*C* (9 mm)	2.93	4.70	4.69
4,5 AGeV, *C*+*Al* (12 mm)	3.58	4.98	3.60
4.5 AGeV, *C*+*Cu* (5 mm)	5.30	7.21	3.06
4.5 AGeV, *C*+*Pb* (10 mm)	2.33	2.58	0.84

Λ hyperon selection criteria:

- Each track has at least 4 hits in Si and GEM detectors (7 detectors in total), where hit is a combination of two strip clusters on both readout sides (X and X' views) on each detector [GEMTDR]
- Momentum range of positive tracks: $p_{pos} < 3.9$, 4.4 GeV/c for 4.0 and 4.5 AGeV carbon beam data, respectively
- Momentum range of negative tracks: $p_{neg} > 0.3$ GeV/c
- Distance of the closest approach of *V0* decay tracks (distance in X-Y plane between *V0* decay tracks at $Z=Z_{V0}$): $dca < 1$ cm
- Distance between *V0* and primary vertex: $path > 2.0$-2.5 cm

Distributions of the experimental primary vertex are given in Fig.6. Distributions of kinematic and spatial parameters used for the Λ hyperon selection are presented in Fig.7.

Λ hyperon signal in data:

Spectra of the invariant mass of (p,π^-) reconstructed in interactions of 4.0 and 4.5 AGeV carbon beam with different targets are shown in Fig.10a and 10b, respectively. To extract Λ hyperon signal, the distributions were fitted to the 4th degree Legendre polynomial (background) in the mass range 1.08-1.18 GeV/c^2. To avoid a bias due to possible deviation of the peak from the Gaussian shape, the numbers of Λ hyperons were determined not from the Gaussian fit but from the content of the background-subtracted histogram bins within 1107.5-1125 MeV/c^2 mass window. This mass window where Λ signal contributes was excluded from the Legendre polynomial fit. Λ signals in intervals of the transverse momentum p_T and rapidity y_{lab} were reconstructed using similar fit procedure, i.e. the numbers of Λ hyperons were calculated within 1107.5-1125 MeV/c^2 window as excess signals relative to background calculated from fits of (p,π^-) mass spectra to the 4th Legendre polynomial in p_T and y_{lab} intervals. The error of the Λ signal includes the uncertainty of the background subtraction. The statistical and systematic errors were calculated according to the formula: $sig = hist - bg$, $err(stat) = \sqrt{hist}$, $err(syst) = \sqrt{(0.5*bg)}$, assuming that the background was estimated with the uncertainty of $\sqrt{(0.5*bg)}$. If the variation of the background shape due to use of the 3th degree Legendre polynomial gave larger uncertainties than $\sqrt{(0.5*bg)}$, the largest uncertainty was taken as a systematic error. The statistics of Λ hyperons reconstructed in *C+C, C+Al, C+Cu, C+Pb* interactions in bins of y_{lab} and p_T are summarized in Fig.11a,b and in Tables 3a and 3b for 4.0 AGeV and 4.5 AGeV carbon beam data, respectively.

Table 3a. Reconstructed signals of Λ hyperons in bins of y_{lab} and p_T in 4.0 AGeV carbon-target interactions. The first error presents the statistical uncertainty, the second error is systematic.

Target / *y* inter. in lab. frame	**Y**				Target / p_T interval	p_T			
	C	***Al***	***Cu***	***Pb***		***C***	***Al***	***Cu***	***Pb***
1.2-1.45	225±35±23	279±52±35	610±66±43	133±27±18	0.1-0.3	463±58±38	427±77±52	691±89±60	164±35±23
1.45-1.65	343±41±26	475±61±40	643±73±48	110±28±19	0.3-0.55	380±52±34	538±76±51	787±89±60	159±34±22
1.65-1.85	334±48±31	420±69±46	604±79±54	102±31±20	0.55-0.8	285±40±25	462±61±40	450±70±47	91±27±18
1.85-2.1	284±52±35	371±72±49	375±79±55	111±30±19	0.8-1.05	57±20±13	118±32±21	304±39±25	43±13±9

Table 3b. Reconstructed signals of Λ hyperons in bins of y_{lab} and p_T in 4.5 AGeV carbon-target interactions. The first error presents the statistical uncertainty, the second error is systematic.

Target y inter. in lab. frame	y				Target p_T interval	p_T			
	C	***Al***	***Cu***	***Pb***		***C***	***Al***	***Cu***	***Pb***
1.25-1.5	170±38±25	316±67±46	640±81±55	292±69±47	0.1-0.3	141±58±40	270±91±63	674±103±70	211±79±55
1.5-1.7	248±42±28	555±76±50	635±87±59	304±69±47	0.3-0.55	306±52±34	632±92±63	803±104±71	418±81±56
1.7-1.9	242±48±32	570±84±56	626±93±64	417±70±48	0.55-0.8	239±43±28	549±79±53	698±88±60	312±69±47
1.9-2.15	79±54±37	223±91±62	650±98±67	57±70±49	0.8-1.05	54±24±16	211±48±32	375±55±36	129±43±28

Event simulation:

To evaluate the Λ hyperon acceptance and reconstruction efficiencies, minimum bias interactions of 4.0 and 4.5A GeV carbon beam with *C, Al, Cu, Pb* targets were generated with the DCM-QGSM generator. The generated particles were traced through the BM@N geometry using the GEANT simulation and reconstructed using the BmnRoot software framework. Experimental and Monte Carlo distributions of the track multiplicity, number of tracks reconstructed in the primary vertex and number of hits per track are presented in Fig.2a and 2b for 4.0 and 4.5 AGeV carbon beam data, respectively. Distributions of the transverse momentum p_T and total momentum p of reconstructed positive and negative particles in data and simulation are shown in Fig.3a and 3b for interactions of 4.0 and 4.5 AGeV carbon beam, respectively.

To reproduce the detector effects in the reconstruction efficiency the simulated products of Λ hyperon decays (p,π^-) were embedded into real experimental events of *C+C, C+Al, C+Cu, C+Pb* interactions. Simulated amplitude signals in the Forward Silicon and GEM detectors were convoluted with amplitudes of the experimental signals in these detectors. Two-dimensional *X/Y* efficiency distributions in 6 GEM stations measured with reconstructed experimental tracks are shown in Fig.4. For each station they were estimated using the following approach:

1. Select good quality tracks with the number of hits per track (excluding the station under study) not less than *N*;
2. Check that track crosses the detector area, if yes, add one track to the denominator;
3. If there is a hit in the detector, which belongs to the track, add one track to the numerator;
4. Detector efficiency = sum of tracks in numerator / sum of tracks in denominator.

These efficiencies were applied to reduce the number of hits of embedded tracks of Λ decay products.

The experimental distribution of GEM hit residuals to tracks is presented in Fig.5. The corresponding distribution for embedded tracks of Λ decay products is also shown in Fig 5. The RMS of distributions are in a reasonable agreement. The invariant mass spectrum of (p,π^-) pairs reconstructed in the experimental events of *C+Cu* interactions with embedded Λ hyperon decay products is illustrated in Fig.8. The Λ signal is reproduced by a Gaussian function with the sigma of 2.4 MeV, which is consistent with the sigma of the experimental Λ distribution of 2.6 MeV. Variation of sigma of the experimental Λ signal and embedded Λ signal reconstructed in bins of p_T is illustrated in Fig.9. To estimate statistical fluctuations of the experimental Λ signal, the Legendre polynomial fit is performed for the mass distribution shifted at a half of the mass bin (1.25 MeV/c^2). The difference in sigma is presented as error bands in the plots.

Λ reconstruction efficiency:

The resulting Λ reconstruction efficiency is the ratio of the number of reconstructed Λ hyperons to the number of generated ones in the intervals of (p_T,y), where y is measured in the laboratory frame (y_{lab}). The reconstruction efficiency can be decomposed into the following components: $\varepsilon_{rec} = \varepsilon_{acc} \cdot \varepsilon_{emb+cuts}$.. The definition of every term is given in Table 4 and their determination procedure is as follows.

Reconstructed primary vertices from experimental events were taken to serve as the interaction point for DCM-QGSM generated events with produced Λs. After the event simulation and reconstruction the successfully reconstructed Λ was counted in the numerator N_{rec} and the procedure continued with the next experimental event. In the opposite case, the current vertex was used for the next MC event. The "successful reconstruction" means that the reconstructed Λ mass was within ±5 MeV window around the table value and the reconstructed hyperon "matches" with the generated one, i.e. its momentum components are within ±0.1 and ±0.15 GeV/c window from the true ones for p_x (p_y) and p_z, respectively, and rapidity within ±0.2. The detector acceptance was taken as N_{rec} / N_{gen}, where N_{gen} is the total number of MC events tried.

The accepted hyperons were used for the embedding procedure as follows. Monte Carlo digits originated from Λ decay products were added to respective experimental events (as explained above) and the reconstruction was performed again for such mixed data. This allowed us to take into account many real-life effects (GEM efficiency, zero suppression, event pile-up). A fraction of successfully reconstructed (in the explained above sense) embedded Λ after applying kinematic and spatial cuts gave the “embedding and selection cuts” efficiency with respect to the number of accepted ones from above.

Table 4. Decomposition of the Λ hyperon reconstruction efficiency.

Reconstruction efficiency	$\varepsilon_{rec} = \varepsilon_{acc} \cdot \varepsilon_{emb+cuts}$
Λ geometrical acceptance in GEM detectors	$\varepsilon_{acc} = N_{acc}(y,p_T) / N_{gen}(y,p_T)$
Efficiency of reconstruction of embedded Λ after applying kinematic and spatial cuts	$\varepsilon_{emb+cuts} = N_{emb+cuts}(y,p_T) / N_{acc}(y,p_T)$

To get 1-dimentional distributions of the full reconstruction efficiency in bins of p_T (y) the summation is done over y (p_T) bins according to the formulae:

$$\varepsilon_{rec}(p_T) = \Sigma_y N_{rec}(y,p_T) / \Sigma_y(N_{rec}(y,p_T)/ \varepsilon_{rec}(y,p_T))$$

$$\varepsilon_{rec}(y) = \Sigma_{pT} N_{rec}(y,p_T) / \Sigma_{pT}(N_{rec}(y,p_T)/ \varepsilon_{rec}(y,p_T))$$

The same approach is used to calculate 1-dimentional distributions of the acceptance and “embedding and selection cuts” efficiency. The actual values of the efficiencies (ε_{acc}, $\varepsilon_{emb+cuts}$) and combined reconstruction efficiencies ε_{rec} calculated in the y and p_T bins are shown in Figs. 12a and 12b for 4.0 AGeV $C+C$ and $C+Cu$ interactions, respectively.

Trigger efficiency:

The trigger efficiency ε_{trig} calculated for events with reconstructed Λ hyperons in interactions of carbon beam with different targets is given in Table 5. The trigger efficiency was evaluated by a convolution of the GEANT simulation of the trigger BD detector response to DCM-QGSM events with reconstructed Λ hyperons and the GEANT simulation of delta electrons produced by the carbon beam in the *C, Al, Cu, Pb* targets which were found to be the dominant source of delta electrons. The dependence of the trigger efficiency on the collision impact parameter is presented in Fig.12c for interactions of the carbon beam with the *C, Al, Cu, Pb* targets. The systematic errors in Table 5 cover: 1) the contribution of delta electrons background produced in the simulated targets with the fractional thickness from 0.5 to 1 of the real targets; 2) the spread of the trigger efficiency values calculated for different y and p_T bins of reconstructed Λ hyperons; 3) change in the trigger efficiency after adjustment (reweighting) of the simulated track multiplicity to the experimental distributions shown in Fig. 2a,b. The trigger efficiency obtained in simulation was cross checked by the analysis of data samples with the reduced trigger requirements: BD>=1 for *C+C* interactions and BD>=2 for *C+Al* and *C+Cu* interactions. The evaluated efficiencies for events with reconstructed Λ ε(BD>=2)/ε(BD>=1,*C+C*) = 0.90, ε(BD>=3)/ε(BD>=2,*C+Al*,*C+Cu*) = 0.95 are consistent with the trigger efficiencies calculated using simulated events.

Table 5. Trigger efficiency evaluated for events with reconstructed Λ hyperons in interactions of the carbon beam with *C, Al, Cu, Pb* targets. The last row shows the trigger efficiency averaged over the data samples with trigger conditions BD>=2 and BD>=3.

Trigger / Target, 4.0 AGeV	***C***	***Al***	***Cu***	***Pb***
ε_{trig} (BD>=2)	0.80±0.02			
ε_{trig} (BD>=3)		0.87±0.02	0.92±0.02	0.95±0.02

Trigger / Target, 4.5 AGeV	***C***	***Al***	***Cu***	***Pb***
ε_{trig} (BD>=2)	0.80±0.02			
ε_{trig} (BD>=3)		0.83±0.02	0.91±0.02	0.94±0.02

Impact parameter distribution:

Distributions of the impact parameters of minimum bias interactions generated with the DCM-QGSM, UrQMD and PSHD models are shown in Fig.12d. The impact parameter distributions of generated events with Λ hyperons as well as the impact parameters of simulated events with reconstructed Λ hyperons are presented for comparison. The Λ reconstruction requirements and the trigger conditions do not change much the impact parameter distributions. The mean values of the impact parameters for events with Λ hyperons generated in *C+C, C+Al, C+Cu, C+Pb* interactions by the DCM-QGSM model are presented in Table 6.

Table 6. Mean impact parameters of min. bias *C+C, C+Al, C+Cu* and *C+Pb* interactions generated by the DCM-QGSM model.

MC	***b*, fm (*C+C*)**	***b*, fm (*C+Al*)**	***b*, fm (*C+Cu*)**	***b*, fm (*C+Pb*)**
All min bias events	3.76	4.36	5.13	6.6
Events with Λ	2.80	3.08	3.58	4.8

Events with rec. Λ	2.71	3.18	3.88	5.2

Evaluation of Λ hyperon cross sections and spectra:

The inclusive cross section σ_Λ and yield Y_Λ of Λ hyperon production in *C+C, C+Al, C+Cu, C+Pb* interactions are calculated in bins of y (p_T) according to the formulae:

$$\sigma_\Lambda(y) = \Sigma y\ [N_{rec}^{\Lambda}(y,p_T) / (\varepsilon_{rec}(y,p_T) \cdot \varepsilon_{trig} \cdot \varepsilon_{pileup} \cdot L)] \qquad Y_\Lambda(y) = \sigma_\Lambda(y) / \sigma_{inel}$$

$$\sigma_\Lambda(p_T) = \Sigma p_T\ [N_{rec}^{\Lambda}(y,p_T) / (\varepsilon_{rec}(y,p_T) \cdot \varepsilon_{trig} \cdot \varepsilon_{pileup} \cdot L)] \qquad Y_\Lambda(p_T) = \sigma_\Lambda(p_T) / \sigma_{inel}$$

where L is the luminosity (Table 2), N_{rec}^{Λ}–the number of reconstructed Λ hyperons (Tables 3a,3b), ε_{rec}–the combined efficiency of the Λ hyperon reconstruction, ε_{trig}–the trigger efficiency (Table 5), ε_{pileup}–the beam halo and pile-up suppression factor (Table 1), σ_{inel}–the cross section for minimum bias inelastic *C+A* interactions (Table 7). The cross section for inelastic C+C interactions is taken from the measurement [AngelovCC]. The cross sections for inelastic *C+Al, C+Cu, C+Pb* interactions are taken from the predictions of the DCM-QGSM model which are consistent with the results calculated by the formula: $\sigma_{inel} = \pi R_0^2 (A_P^{1/3} + A_T^{1/3})^2$, where R_0 = 1.2 fm is an effective nucleon radius, A_P and A_T are atomic numbers of the beam and target nucleus [HadesL0]. The uncertainties for *C+Al, C+Cu, C+Pb* inelastic cross sections are estimated by using the alternative formula: $\sigma_{inel} = \pi R_0^2 (A_P^{1/3} + A_T^{1/3} - b)^2$ with R_0 = 1.46 fm and b = 1.21 [AngelovCC].

Table 7. Inelastic cross sections for carbon-nucleus interactions.

Interaction	***C+C***	***C+Al***	***C+Cu***	***C+Pb***
Inelastic cross section, mb	830±50	1260±50	1790±50	3075±50

The yields of Λ hyperons in minimum bias *C+C, C+Al, C+Cu, C+Pb* interactions are measured in the kinematic range on the Λ transverse momentum of $0.1<p_T<1.05$ GeV/*c* and the Λ rapidity in the laboratory frame of $1.2<y_{lab}<2.1$ for 4.0 AGeV data ($1.25<y_{lab}<2.15$ for 4.5 AGeV data). The rapidity of the beam-target nucleon-nucleon CM system calculated for an interaction of the carbon beam with the kinetic energy of 4.0 (4.5) GeV/nucleon with a fixed target is y_{CM}=1.17 (1.22). The Λ rapidity range for 4.5 AGeV data is shifted at +0.05 to get approximately the same y^* range in the CM system as for 4.0 AGeV data. The transformation of the y distribution to c.m.s. gives $y^*=y_{lab}-y_{CM}$. The differential spectra of the Λ yields in y_{lab} are measured in the Λ transverse momentum range of $0.1<p_T<1.05$ GeV/c. The corrected differential y^* spectra of Λ hyperon yields are presented in Figs. 13a and 13b for 4.0 AGeV and 4.5 AGeV carbon beam energies, respectively. The corrected differential p_T spectra of Λ hyperon yields are presented in Figs. 14a and 14b. The predictions of the DCM-QGSM, URQMD and PHSD models are shown for comparison. In Fig.15a and 15b the measured spectra of the Λ yields in p_T are parameterized by the form: $1/p_T \cdot d^2N/dp_T dy = N \cdot exp(-(m_T - m_\Lambda)/T)$, where $m_T = \sqrt{(m_\Lambda^2 + p_T^2)}$ is the transverse mass, the normalization N and the inverse slope parameter T are free parameters of the fit, dy corresponds to the measured y_{lab} range. The experimental Λ spectra are compared with the predictions of the DCM-QGSM, URQMD and PHSD models. The fit results are consistent within the uncertainties with the predictions of the models. The values of the inverse slope T_0, extracted from the fit of the p_T spectra, are summarized in Table 8.

Table 8. Inverse slope parameter extracted from the fit of the p_T spectra.

4.0 AGeV	***T_0*, MeV (*C+C*)**	***T_0*, MeV (*C+Al*)**	***T_0*, MeV (*C+Cu*)**	***T_0*, MeV (*C+Pb*)**
Experiment χ^2 / ndf	95 ± 11 ± 9 1.61/2	119 ± 15 ± 12 0.20/2	125 ± 11 ± 9 1.27/2	130 ± 25 ± 21 0.36/2
DCM-QGSM	126	120	133	130
UrQMD	107	128	133	136
PHSD	87	100	105	98

4.5 AGeV	***T_0*, MeV (*C+C*)**	***T_0*, MeV (*C+Al*)**	***T_0*, MeV (*C+Cu*)**	***T_0*, MeV (*C+Pb*)**
Experiment χ^2 / ndf	114 ± 16 ± 12 3.07/2	137 ± 19 ± 15 1.49/2	122 ± 13 ± 11 1.30/2	129 ± 24 ± 19 0.77/2
DCM-QGSM	132	133	135	142
UrQMD	122	128	130	134
PHSD	101	106	109	108

Systematic uncertainties:

The systematic error of the Λ yield in every p_T and y bin is calculated via a quadratic sum of uncertainties coming from the following sources:

- Systematic errors of the embedding efficiency estimated by embedding the Λ decay products into data samples collected in different run periods.
- Systematic errors of the background subtraction under Λ signal in the (p,π^-) invariant mass spectra (see text above).
- The Λ yield normalization uncertainty calculated as a quadratic sum of uncertainties of the trigger efficiency, luminosity and inelastic cross section.

The systematic uncertainties are summarized in Tables 10 and 11.

Table 10. Total systematic uncertainty of the Λ yield for 4.0 AGeV

Target / Interval	***y***				Target / Interval	***p_T***			
	C sys%	***Al*** sys%	***Cu*** sys%	*Pb* sys%		***C*** sys%	***Al*** sys%	***Cu*** sys%	***Pb*** sys%
1.2-1.45	11.4	14.5	8.6	16.8	0.1-0.3	10.0	13.6	10.0	15.8
1.45-1.65	9.3	9.6	8.2	16.4	0.3-0.55	9.7	10.8	7.7	14.3
1.65-1.85	11.0	13.1	10.7	20.1	0.55-0.8	10.5	11.5	11.5	15.3
1.85-2.1	15.0	16.1	18.9	22.3	0.8-1.05	28.9	25.9	23.3	34.5
Normalization	4.9	3.8	3.0	3.0	Normalization	4.9	3.8	3.0	3.0

Table 11. Total systematic uncertainty of the Λ yield for 4.5 AGeV.

Target / Interval	***y***				Target / Interval	***p_T***			
	C, sys%	***Al***, sys%	***Cu***, sys%	***Pb***, sys%		***C***, sys%	***Al***, sys%	***Cu***, sys%	***Pb***, sys%
1.25-1.5	15.4	16.3	13.1	16.5	0.1-0.3	24.5	22.8	13.3	23.4
1.5-1.7	13.3	10.4	10.8	15.0	0.3-0.55	12.1	12.4	10.7	14.3
1.7-1.9	14.6	11.9	11.5	12.6	0.55-0.8	11.6	11.3	13.4	16.7

1.9-2.15	27.8	29.0	12.4	29.1	0.8-1.05	40.3	16.4	15.5	22.8
Normalization	4.9	3.8	3.0	3.0	Normalization	4.9	3.8	3.0	3.0

Integrated yields and cross sections:

The integrated yields of *Λ* hyperons produced in the kinematic range of $0.1<p_T<1.05$ GeV/*c* and $1.2<y_{lab}<2.1$ ($1.25<y_{lab}<2.15$ for 4.5 AGeV data) in minimum bias *C+C, Al, Cu, Pb* interactions are summarized in Tables 12a and 12b. To extrapolate the measured yields to the full kinematic range the predictions of the DCM-QGSM and URQMD models are used. The model extrapolation factors, reconstruction efficiencies, the inverse slopes extracted from fits to the invariant p_T spectra, the estimated yields and inclusive cross sections of the *Λ* hyperon production in *C+C, C+Al, C+Cu, C+Pb* minimum bias interactions with beam energies of 4.0 and 4.5 AGeV are also given in Tables 12a and 12b.

Table 12a. Extrapolation factors to the full kinematic range, reconstruction efficiencies, *Λ* hyperon yields and cross sections for 4.0 AGeV data. The first error given is statistical, the second error is systematic.

4.0 AGeV	***C***	***Al***	***Cu***	***Pb***
DCM-QGSM URQMD extrap. factor (average)	2.76	3.08	4.23	6.17
Efficiency in $0.1<p_T<1.05$ GeV/c, $1.2<y_{lab}<2.1$	0.027	0.027	0.024	0.021
Yields in $0.1<p_T<1.05$ GeV/c, $1.2<y_{lab}<2.1$	0.0164±0.0013±0.0010	0.0286±0.0025±0.0020	0.0307±0.0020±0.0016	0.0366±0.0048±0.0036
Yields in the full kin. range *Npart / Ncoll* DCM-QGSM	0.0453±0.0036±0.0027 9 / 5	0.0882±0.0077±0.0060 13.4 / 9.3	0.131±0.009±0.007 23 / 18	0.226±0.030±0.023 50.5 / 52.5
Λ cross section in min. bias interact, mb	37.6 ± 3.0 ± 2.3	111.2 ± 9.7 ± 7.6	234 ± 16 ± 12	695 ± 91 ± 72
Inverse slope parameter, MeV / $\chi2$ / ndf	95 ± 11 ± 9 1.61/2	119 ± 15 ± 12 0.20/2	125 ± 11 ± 9 1.27/2	125 ± 25 ± 21 0.36/2

Table 12b. Extrapolation factors to the full kinematic range, reconstruction efficiencies, *Λ* hyperon yields and cross sections for 4.5 AGeV data. The first error given is statistical, the second error is systematic.

4.5 AGeV	***C***	***Al***	***Cu***	***Pb***
DCM-QGSM URQMD extrap. factor (average)	2.48	3.07	3.98	6.74
Efficiency in	0.020	0.021	0.016	0.014

$0.1<p_T<1.05$ GeV/c, $1.25<y_{lab}<2.15$				
Yields in $0.1<p_T<1.05$ GeV/c, $1.25<y_{lab}<2.15$	0.0224±0.0026±0.0019	0.0355±0.0034±0.0026	0.0406±0.0032±0.0026	0.040±0.0057±0.0043
Yields in the full kin. range *Npart* / *Ncoll* DCM-QGSM	0.0554±0.0064±0.0047 9 / 5	0.109±0.010±0.008 13.4 / 9.3	0.164±0.013±0.011 23 / 18	0.273±0.038±0.029 50.5 / 52.5
Λ cross section in min. bias interact., mb	46.0 ± 5.3 ± 3.9	137 ± 13 ± 10	293 ± 23 ± 19	839 ± 117 ± 90
Inverse slope parameter, MeV / χ^2 / ndf	114 ± 16 ± 12 3.07/2	137 ± 19 ± 15 1.49/2	122 ± 13 ± 11 1.30/2	129 ± 24 ± 19 0.77/2

Table 12c. *Λ* hyperon yields and yields normalized to the number of nucleons-participants. The first error is statistical, the second error is systematic. Predictions of the DCM-QGSM, UrQMD and PHSD models are shown for carbon-carbon interactions at different beam energies.

C+C	**4.5 AGeV**	**4.0 AGeV**	**3.5 AGeV**	**2.0 AGeV**
BM@N yield Npart / Ncoll Yield normal to N_{part} Yield normal to N_{coll}	0.0554±0.0064±0.0047 9 / 5 = 1.8 (6.16±0.71±0.52)·10^{-3} (11.1±1.28±0.94)·10^{-3}	0.0453±0.0036±0.0027 (5.03±0.40±0.30)·10^{-3} (9.05±0.72±0.54)·10^{-3}		
DCM-QGSM DCM-QGSM / N_{part} DCM-QGSM / N_{col}	0.1518 16.86·10^{-3} 30.35·10^{-3}	0.1103 12.26·10^{-3} 22.07·10^{-3}	0.0771 8.57·10^{-3} 15.43·10^{-3}	0.0125 1.39·10^{-3} 2.50·10^{-3}
UrQMD yield UrQMD / N_{part} UrQMD / N_{coll}	0.0927 10.3·10^{-3} 18.54·10^{-3}	0.0736 8.17·10^{-3} 14.71·10^{-3}	0.0577 6.41·10^{-3} 11.54·10^{-3}	0.0118 1.31·10^{-3} 2.36·10^{-3}
PHSD yield PHSD / N_{part} PHSD / N_{coll}	0.1167 12.97·10^{-3} 23.35·10^{-3}	0.09 10.0·10^{-3} 18.0·10^{-3}	0.0684 7.6·10^{-3} 13.7·10^{-3}	0.0119 1.32·10^{-3} 2.38·10^{-3}
Other Experiments			(2.89±0.72) ·10^{-2} (3.36 AGeV) (2.8±0.3) ·10^{-2} (3.36 AGeV) Propane Chamber	(0.92±0.12+0.34-0.17) ·10^{-2} HADES

Table 12d. *Λ* hyperon yields and yields normalized to the number of nucleons-participants. The first error is statistical, the second error is systematic. Predictions of the DCM-QGSM, UrQMD and PHSD models are shown for carbon-nucleus interactions at different beam energies.

C+Al	**4.5 AGeV**	**4.0 AGeV**	**3.5 AGeV**
BM@N yield Npart / Ncoll Yield normal to N_{part} Yield normal to N_{coll}	0.109±0.010±0.008 13.4 / 9.3 = 1.441 (8.13±0.75±0.60)·10^{-3} (11.72±1.08±0.86)·10^{-3}	0.0882±0.0077±0.0060 (6.58±0.57±0.45)·10^{-3} (9.48±0.82±0.65)·10^{-3}	
DCM-QGSM QGSM / N_{part} QGSM / N_{coll}	0.2231 16.65·10^{-3} 23.99·10^{-3}	0.164 12.24·10^{-3} 17.64·10^{-3}	0.1153 8.61·10^{-3} 12.41·10^{-3}
UrQMD yield UrQMD / N_{part}	0.1414	0.1138	0.092

UrQMD / N_{coll}	$10.55{\cdot}10^{-3}$	$8.49{\cdot}10^{-3}$	$6.86{\cdot}10^{-3}$
PHSD yield PHSD / N_{part} PHSD / N_{coll}	0.1685 $12.58{\cdot}10^{-3}$	0.1339 $9.99{\cdot}10^{-3}$	0.0983 $7.34{\cdot}10^{-3}$
C+Cu	**4.5 AGeV**	**4.0 AGeV**	**3.5 AGeV**
BM@N yield Npart / Ncoll Yield normal to N_{part} Yield normal to N_{coll}	0.164±0.013±0.011 23 / 18 = 1.278 $(7.13±0.56±0.48){\cdot}10^{-3}$	0.131±0.009±0.007 (5.70±0.39±0.30)·10-3	
DCM-QGSM QGSM / N_{part} QGSM / N_{coll}	0.3279 $14.26{\cdot}10^{-3}$	0.2503 $10.88{\cdot}10^{-3}$	0.1782 $7.75{\cdot}10^{-3}$
UrQMD yield UrQMD / N_{part} UrQMD / N_{coll}	0.2108 $9.16{\cdot}10^{-3}$	0.1732 $7.53{\cdot}10^{-3}$	0.1367 $5.94{\cdot}10^{-3}$
PHSD yield PHSD / N_{part} PHSD / N_{coll}	0.2433 $10.58{\cdot}10^{-3}$	0.1914 $8.32{\cdot}10^{-3}$	0.1445 $6.28{\cdot}10^{-3}$
C+Pb	**4.5 AGeV**	**4.0 AGeV**	**3.5 AGeV**
BM@N yield Npart / Ncoll Yield normal to N_{part} Yield normal to N_{coll}	0.273±0.038±0.029 52.5 / 50.5 = 0.9619 $(5.41±0.75±0.57){\cdot}10^{-3}$	0.226±0.030±0.023 $(4.48±0.59±0.46){\cdot}10^{-3}$	
DCM-QGSM QGSM / N_{part} QGSM / N_{coll}	0.4937 $9.78{\cdot}10^{-3}$	0.3872 $7.67{\cdot}10^{-3}$	0.277 $5.48{\cdot}10^{-3}$
UrQMD yield UrQMD / N_{part} UrQMD / N_{coll}	0.3504 $6.94{\cdot}10^{-3}$	0.2947 $5.84{\cdot}10^{-3}$	0.2215 $4.39{\cdot}10^{-3}$
PHSD yield PHSD / N_{part} PHSD / N_{coll}	0.3798 $7.52{\cdot}10^{-3}$	0.3033 $6.01{\cdot}10^{-3}$	0.2261 $4.48{\cdot}10^{-3}$

In general, the transport models describe the shape of the differential spectra on y^* and p_T, but predict more abundant yields of Λ hyperons than measured in the experiment. The UrQMD model predictions are closer to the experimental data in the normalization than the predictions of the DCM-QGSM and PHSD models. The PHSD model predicts a stronger rise of the Λ hyperon yields in the BM@N kinematic range with the atomic weight of the target than the DCM-QGSM and UrQMD models. This tendency is deduced from the rapidity spectra of Λ hyperons generated in the models which are shown in Fig.12e.

The Λ yields and production cross sections in *C+C* interactions can be compared with the previous results of 23.2±2.5 mb [ArmutCC] and 24±6 mb [ArakelianCC] measured in interactions of the carbon beam with the momentum of 4.2 GeV/*c* per nucleon (beam kinetic energy of 3.36 GeV per nucleon) with the Propane Chamber experiment, as well as with the result of the HADES experiment at 2A GeV. In Fig.16a the BM@N result for the Λ yield in *C+C* minimum bias interactions is compared with the results taken from other experiments [ArakelianCC], [ArmutCC], [HadesL0]. The *C+C* data are compared with predictions of the

DCM-QGSM, UrQMD and PHSD transport models (Fig16a and Table 12c). There is a general tendency that the transport models predict a faster rise of the Λ hyperon yield with the energy in comparison with the experimental data. The energy dependences of the Λ yields measured in BM@N are also presented in Table 12d and Fig.16b,c,d for *C+Al, C+Cu, C+Pb* minimum bias interactions, respectively. The predictions of the transport models are shown. In general, the model predictions exceed the experimental data in the normalization. The DCM-QGSM model predicts a higher full yield of Λ hyperons than the two other models.

Table 13. Yields and inclusive cross sections of Λ hyperon production in interactions of light and medium nucleus.

Interacting nucleus / reference	Beam momentum, kinetic energy (E_{kin})	Λ cross section, mb	Λ yield, $\cdot 10^{-2}$
He_4+Li_6	4.5 GeV/c (3.66A GeV)	5.9± 1.5	1.85 ± 0.5
C+C	4.2 GeV/c (3.36A GeV)	24 ± 4	2.89±0.72
C+C, propane Chamber	4.2 GeV/c (3.36A GeV)	23.2±2.5	2.8 ± 0.3
p+p	4.95 GeV/c (4.1 GeV)		2.3 ± 0.4
C+C, HADES	2A GeV	$8.7\pm1.1\pm^{3.2}_{1.6}$	$0.92\pm0.12\pm^{0.34}_{0.17}$
Ar+KCl, HADES	1.76A GeV		3.93±0.14±0.15
Ar+KCl, FOPI	1.93A GeV		3.9±0.14±0.08
Ni+Ni, FOPI, central 390 mb from 3.1 *b*	1.93A GeV		$0.137\pm0.005\pm^{0.009}_{0.025}$
Ni+Cu, EOS, full *b*<8.9 fm / central *b*<2.4 fm	2A GeV	112±24 / 20±3	
Ar+KCl, central *b*<2.4 fm	1.8A GeV	7.6±2.2	

To compare yields of particle production in nucleus-nucleus interactions, they are usually normalized to the mean number of nucleons participating in interactions (Participants). The numbers of Participants in minimum bias *C+C, C+Al, C+Cu, C+Pb* interactions are estimated using the DCM-QGSM model [GenisPart]. The results (*A1+A2*) are shown in Table 14. The ratios of the Λ hyperon yields to the number of nucleons-participants measured in BM@N carbon-nucleus interactions are presented in Fig.17 and in Tables 12c,d. The ratios reach maximal values of $0.62\cdot10^{-2}$ and $0.76\cdot10^{-2}$ for *C+Al* interactions at 4.0 and 4.5 AGeV, respectively. There is a tendency that the measured ratios are smoothly decreasing for heavier target nuclei. This tendency is also reproduced by the transport model predictions shown in Fig.17.

Table 14. Number of Participants in minimum bias *A+A* events at 4A GeV.

A_1A_2	A_1	A_2	$A_1 + A_2$
C+C	4.5	4.5	9.0
C+Al	5.23	8.14	13.37
C+Cu	6.21	16.79	23.0

C+Pb	7.33	43.15	50.48

Summary

Production of Λ hyperons in interactions of the carbon beam with *C*, *Al*, *Cu*, *Pb* targets was studied with the BM@N detector. The analysis procedure is described including details of the Λ hyperon reconstruction, efficiency and systematic uncertainty evaluation. First physics results are presented on Λ hyperon yield and cross sections in minimum bias carbon-nucleus interactions at the beam kinetic energies of 4.0 and 4.5 AGeV. The results are compared with models of nucleus-nucleus interactions and with the results of other experiments studied carbon-nucleus interactions at lower energies.

Bibliography

[DeuteronPaper] D.Baranov et al., First Results from BM@N Technical Run with Deuteron Beam, Phys. Part. Nucl. Lett. 15, no. 2, 148 (2018)

[GEMconf] http://bmnshift.jinr.ru/wiki/lib/exe/detail.php?id=run_5_december_2016&media=setting_1_f.jpg

[GEMTDR] http://bmnshift.jinr.ru/wiki/lib/exe/fetch.php?media=tdr_gem_may2017_v1.doc

[CBM1] V. Akishina and I. Kisel. Time-based cellular automaton track finder for the CBM experiment - 2015. J. Phys.: Conf. Ser. 599, 012024

[CBM2] S. Gorbunov and I. Kisel. Reconstruction of decayed particles based on the Kalman filter - 2007. CBM-SOFTnote--003

[GenisPart] Result of Genis Musulmanbekov, private communication

[AnikinaCC] N.Anikina et al., Z.Phys.C, 25,(1984),1

[ArmutCC] D.Armutlijsky et al., P1-85-220, JINR, Dubna

[ArakelianCC] S.Arakelian et al., P1-83-354, JINR, Dubna

[AngelovCC] H.Angelov et al., P1-80-473, JINR, Dubna

[HadesL0] Kalliopi Kanaki, PhD “Study of Λ hyperon production in *C+C* collisions at 2A GeV beam energy with the HADES spectrometer”, 2007

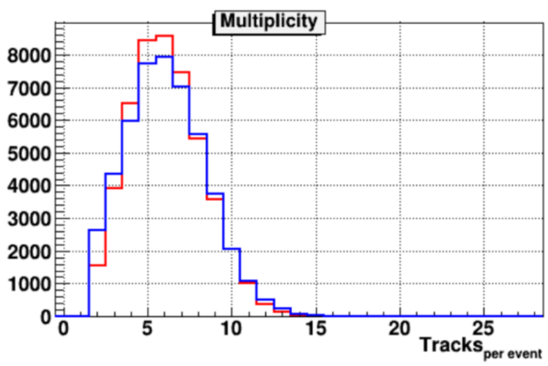

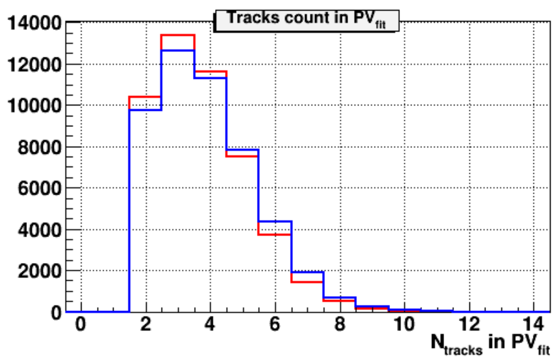

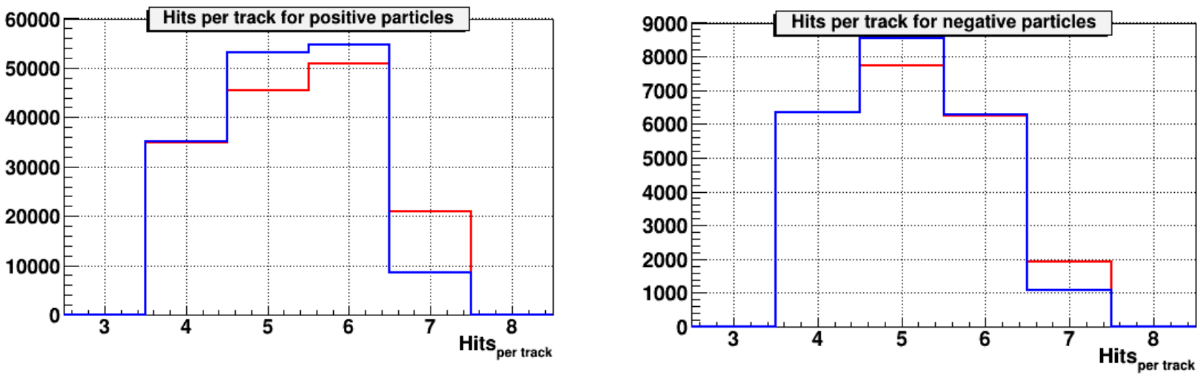

Fig.2a. *C+Cu* interactions at 4.0 AGeV carbon beam energy: comparison of experimental distributions (red lines) and Monte Carlo GEANT distributions of events generated with the DCM-QGSM model (blue lines): track multiplicity per event; number of tracks reconstructed in the primary vertex; number of hits per positive particle reconstructed in 1 Si + 6 GEM detectors; number of hits per negative particle.

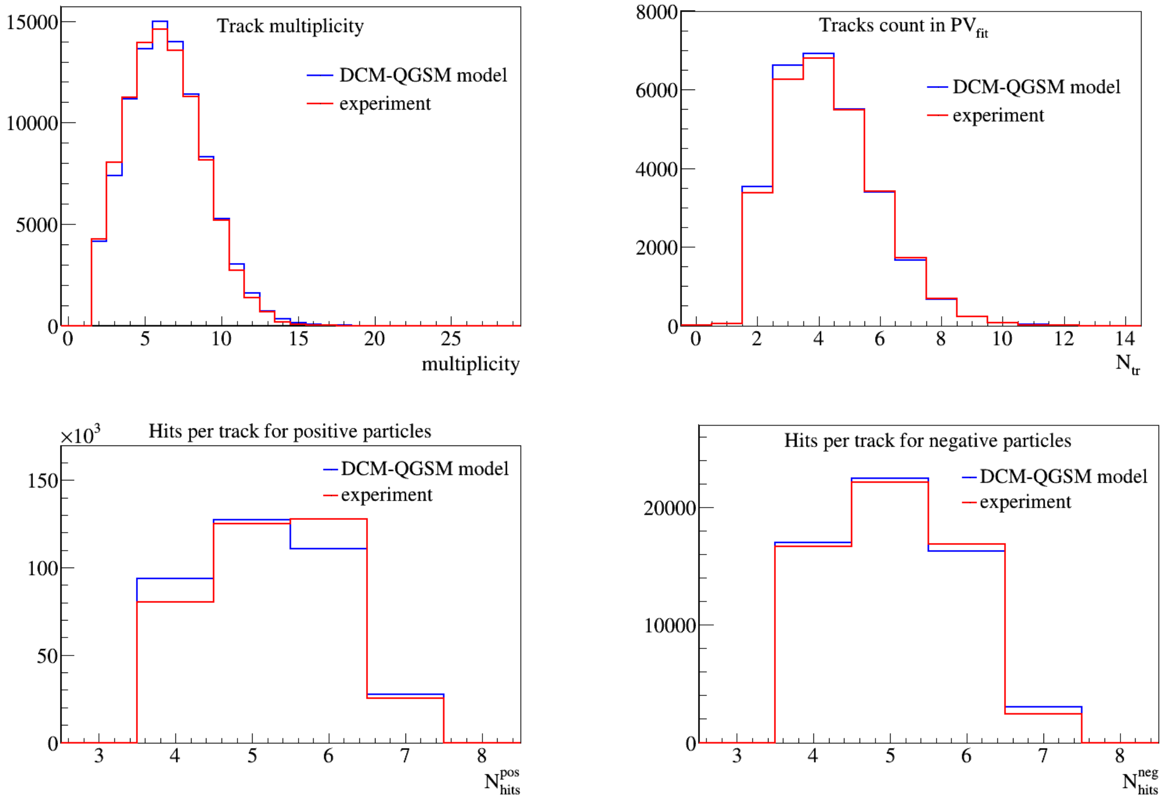

Fig.2b. *C+Cu* interactions at 4.5 AGeV carbon beam energy: comparison of experimental distributions (red lines) and Monte Carlo GEANT distributions of events generated with the DCM-QGSM model (blue lines): track multiplicity per event; number of tracks reconstructed in the primary vertex; number of hits per positive particle reconstructed in 1 Si + 6 GEM detectors; number of hits per negative particle.

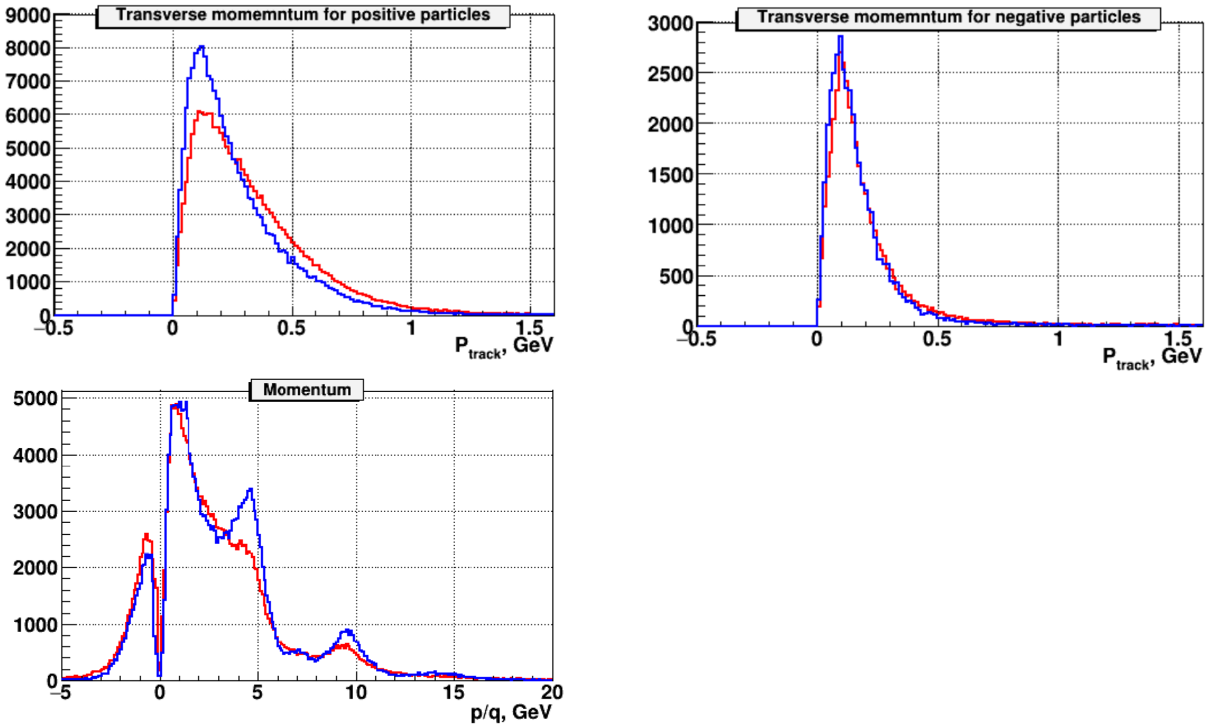

Fig. 3a. *C+Cu* interactions at 4.0 AGeV carbon beam energy: comparison of experimental data (red curves) and DCM-QGSM + GEANT Monte Carlo simulation (blue curves): transverse momentum of positive particles; transverse momentum of negative particles; total momentum of negative (*p/q*<0) and positive particles (*p/q*>0).

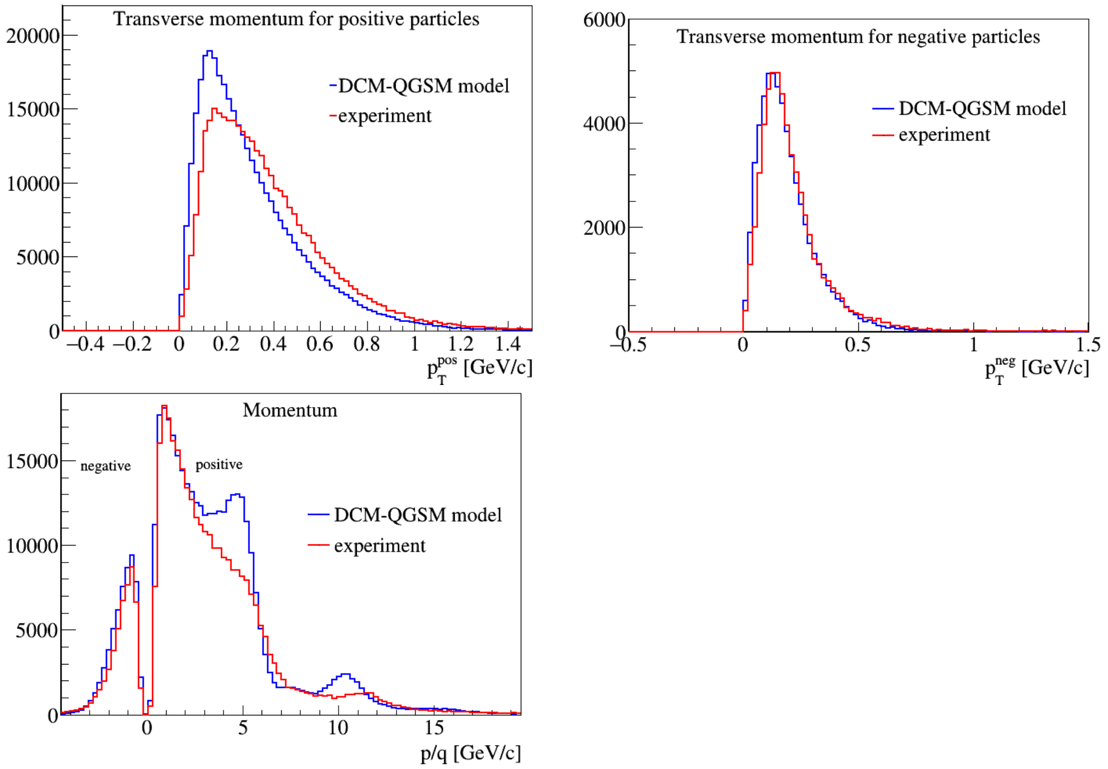

Fig. 3b. *C+Cu* interactions at 4.5 AGeV carbon beam energy: comparison of experimental data (red curves) and DCM-QGSM + GEANT Monte Carlo simulation (blue curves): transverse momentum of positive particles; transverse momentum of negative particles; total momentum of negative (*p/q*<0) and positive particles (*p/q*>0).

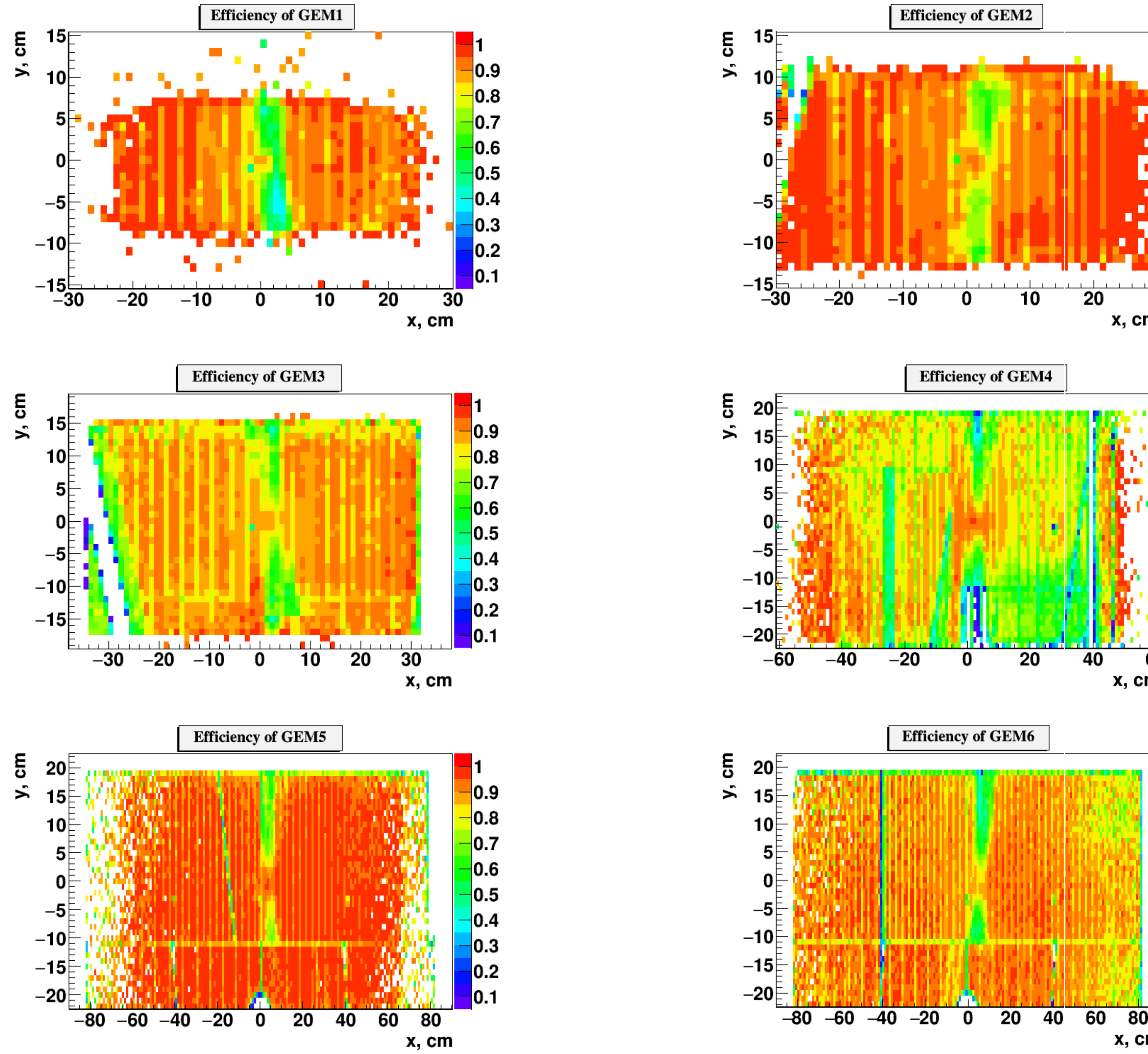

Fig. 4. Two-dimensional *X/Y* efficiency distributions in 6 GEM stations measured with experimental tracks and implemented into Monte Carlo simulation.

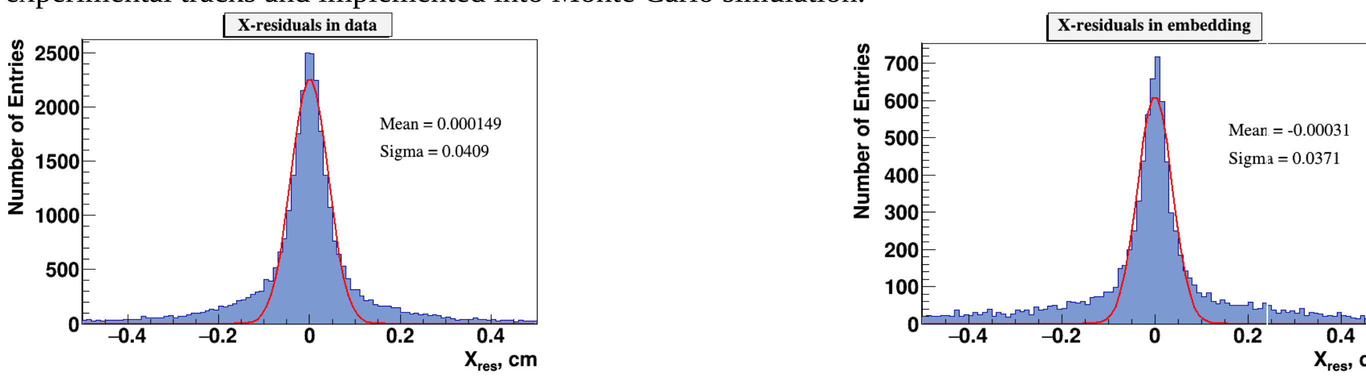

Fig. 5. Residual distributions of GEM hits with respect to reconstructed tracks: left) experimental data, right) reconstructed tracks of embedded *Λ* decay products.

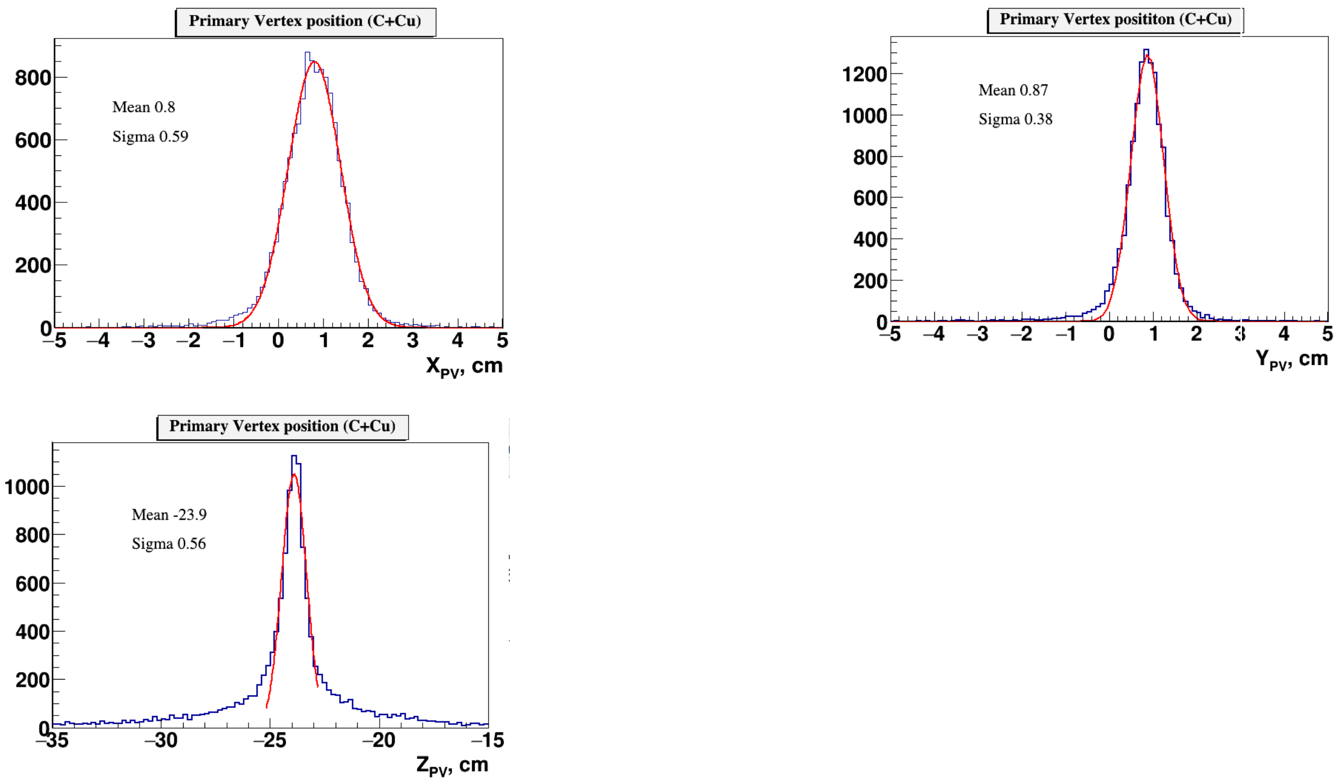

Fig. 6. *X*,*Y*,*Z* distributions of the experimental primary vertex.

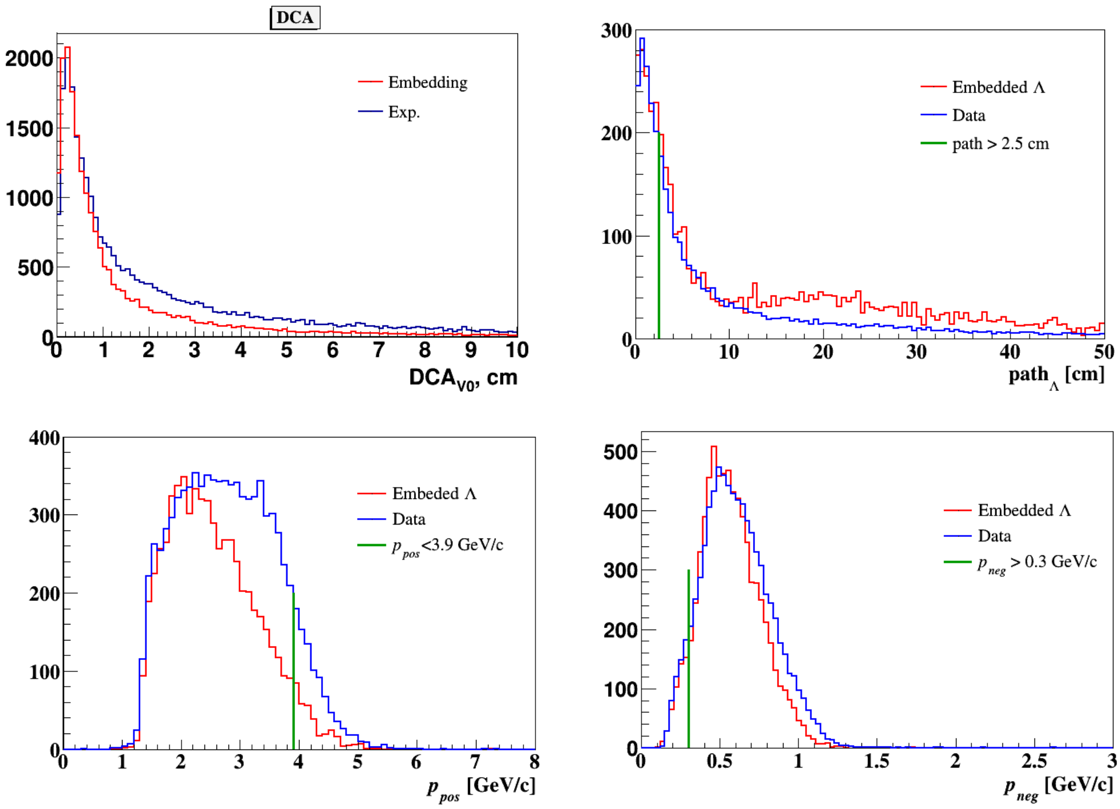

Fig.7. Distance of the closest approach of *V0* decay tracks (*dca*), distance between the primary vertex and *V0* (path), momentum distributions of positive, negative tracks from *V0* decays. Experimental data at 4.0 AGeV carbon beam energy are compared with distributions for embedded *Λ* hyperons.

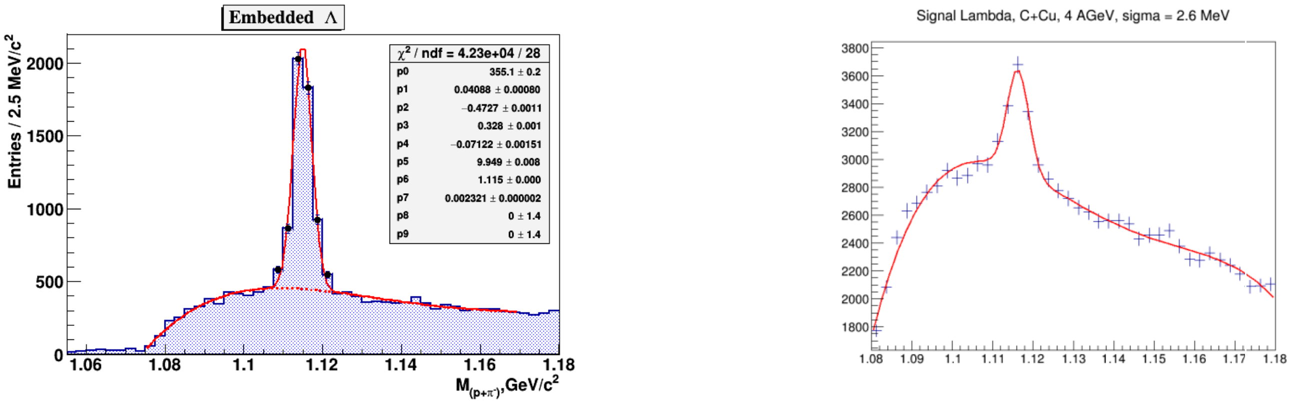

Fig. 8. The invariant mass spectrum of (p,π^-) pairs reconstructed in the experimental events of *C+Cu* interactions at 4.0 AGeV carbon beam energy with embedded Λ hyperon decay products (left); The invariant mass spectrum of (p,π^-) pairs reconstructed in *C+Cu* interactions (right).

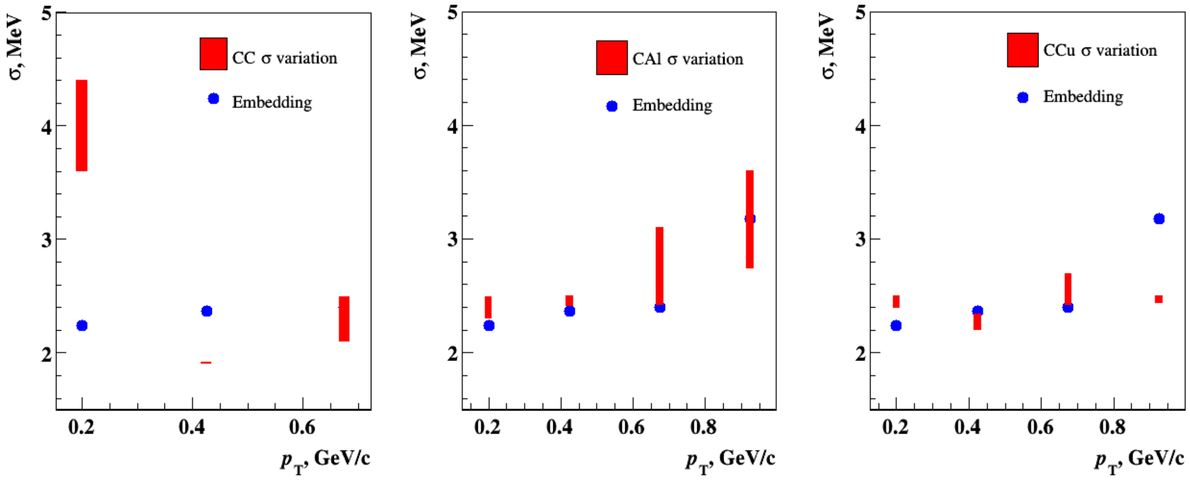

Fig.9. Variation of sigma of the experimental Λ and embedded Λ signals reconstructed in bins of p_T in *C+C*, *C+Al*, *C+Cu* interactions at 4.0 AGeV carbon beam energy. To estimate statistical fluctuations of the experimental Λ signal, the Gaussian fit is performed for the mass distribution shifted at a half of the mass bin (1.25 MeV/c^2). The differences in sigma are presented as error bands.

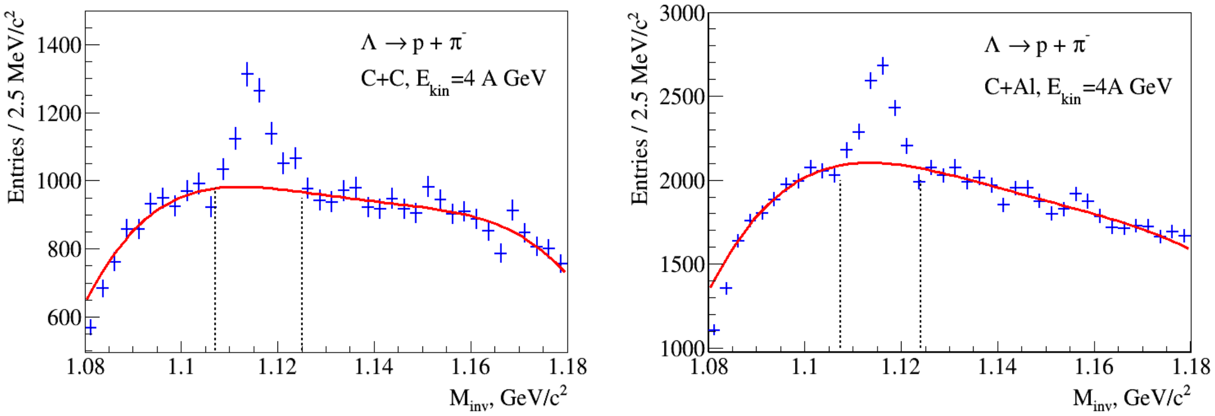

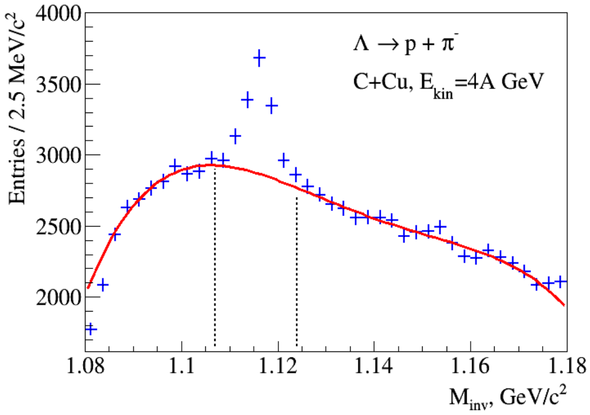

Fig. 10a. *Λ→pπ*⁻ signal reconstructed in *C+C, Al, Cu, Pb* interactions at 4.0 AGeV carbon beam energy. The background is fitted by the 4th degree Legendre polynomial and subtracted from the histogram content in the *Λ* signal mass range indicated by the vertical lines.

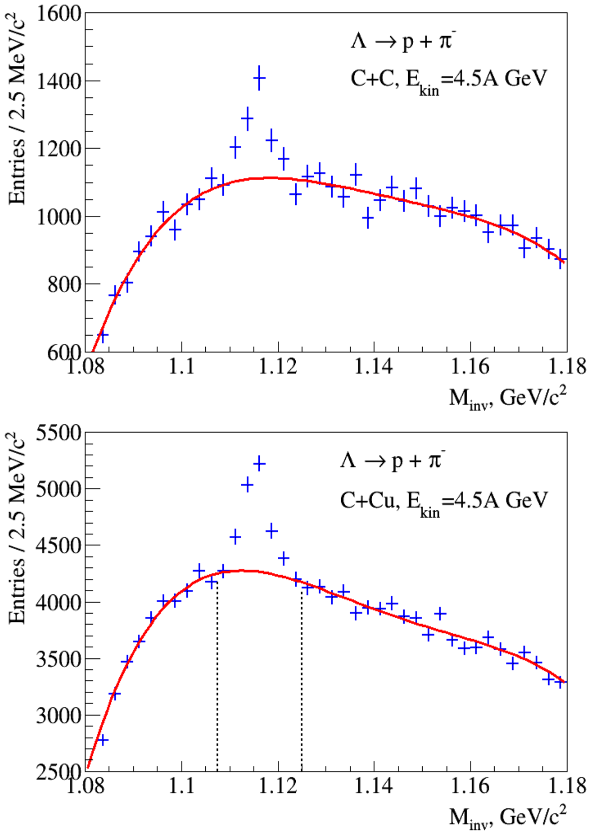

Fig. 10b. *Λ→pπ*⁻ signal reconstructed in *C+C, Al, Cu, Pb* interactions at 4.5 AGeV carbon beam energy. The background is fitted by the 4th degree Legendre polynomial and subtracted from the histogram content in the *Λ* signal mass range indicated by the vertical lines.

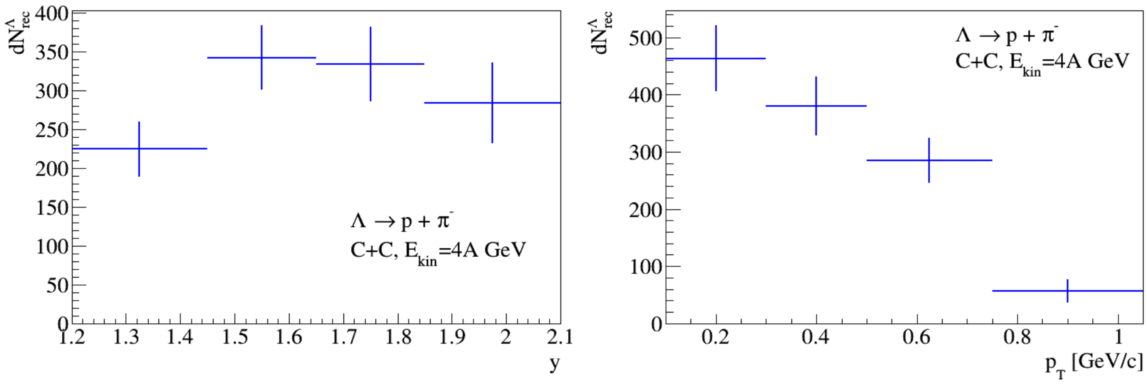

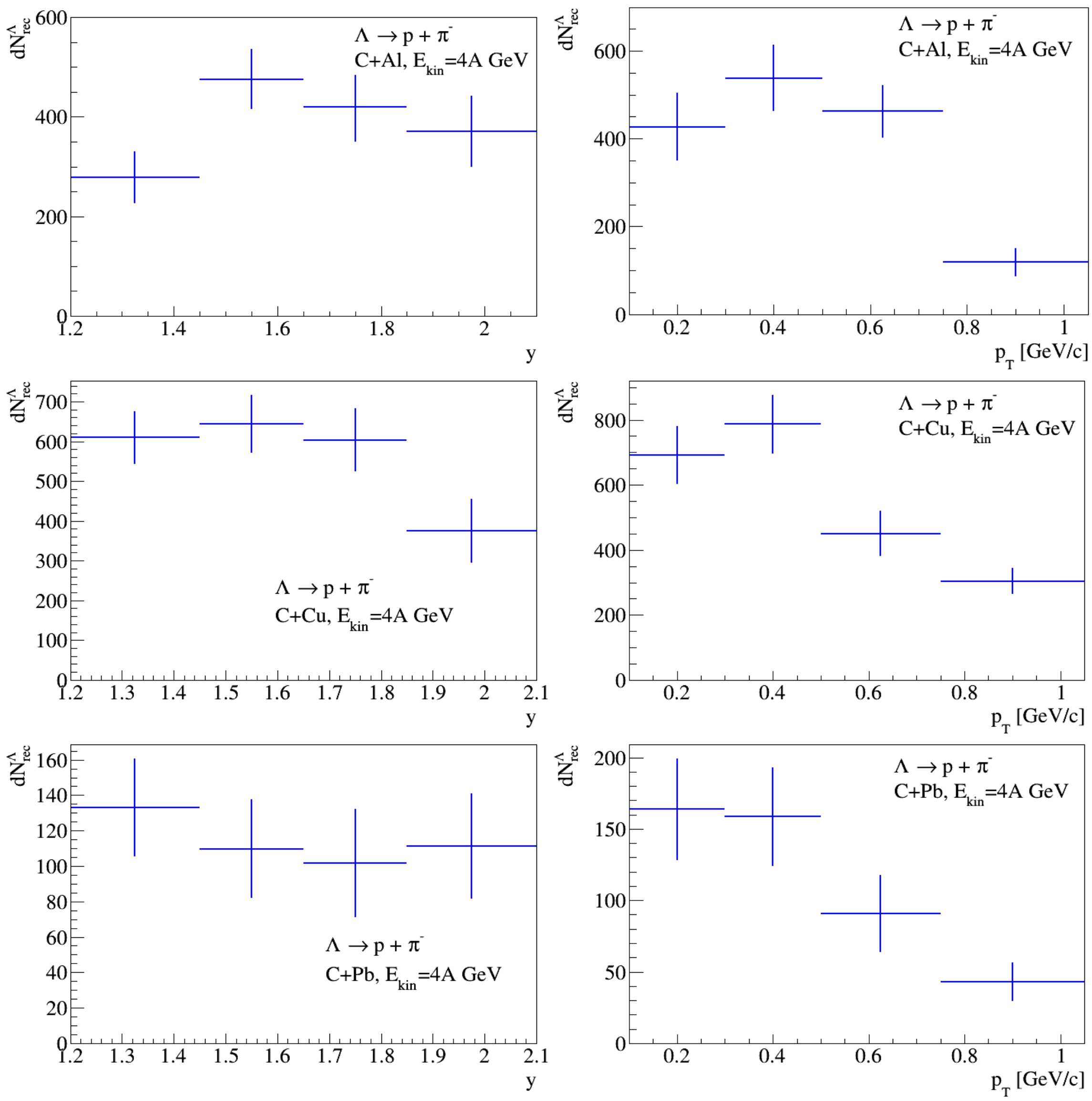

Fig.11a. Number of reconstructed Λ hyperons in interaction of 4.0 AGeV carbon beam with *C*, *Al*, *Cu*, *Pb* targets in bins of y_{lab} and p_T.

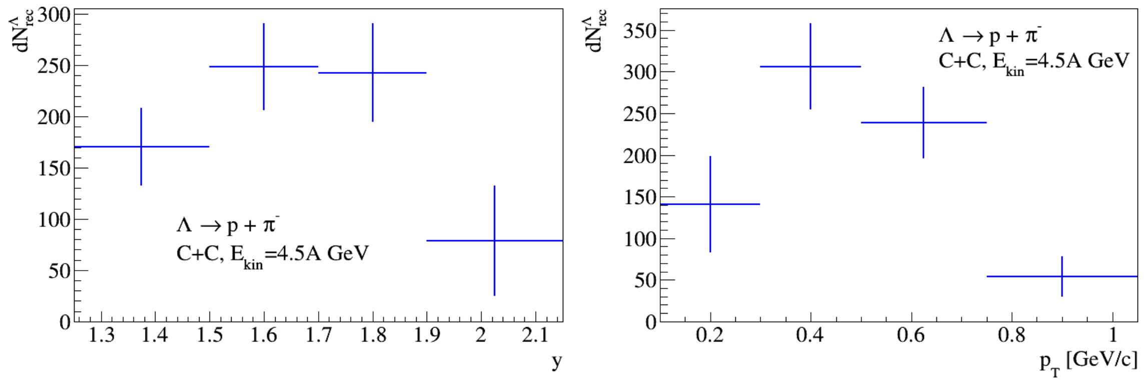

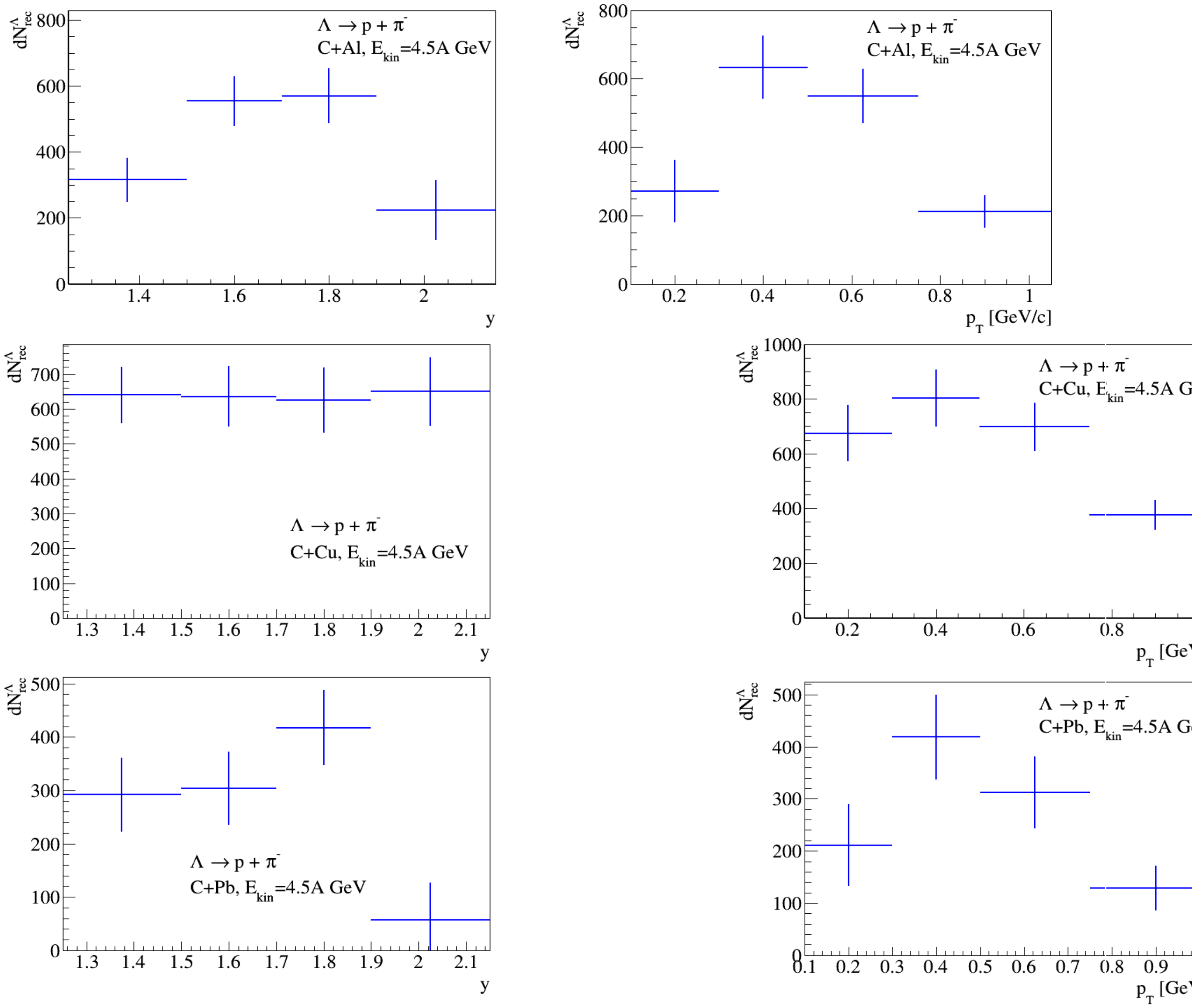

Fig.11b. Number of reconstructed *Λ* hyperons in interaction of 4.5 AGeV carbon beam with *C*, *Al*, *Cu*, *Pb* targets in bins of y_{lab} and p_T.

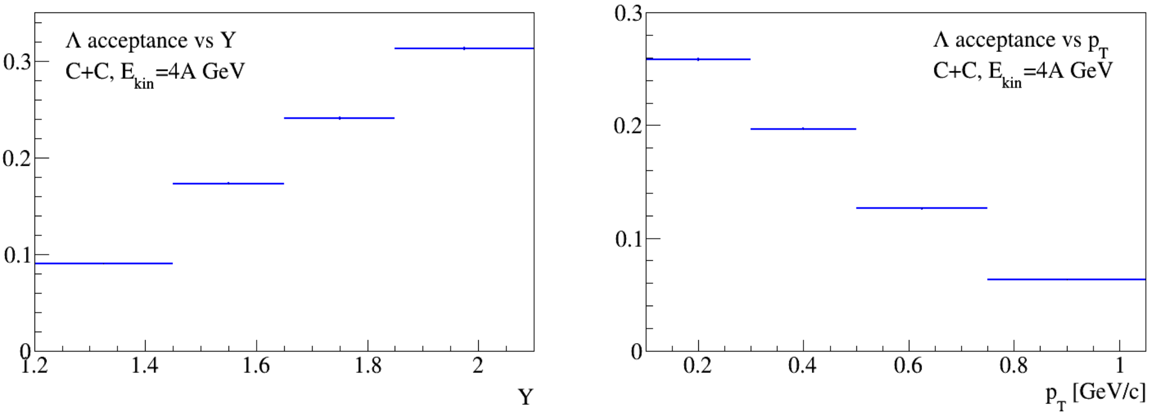

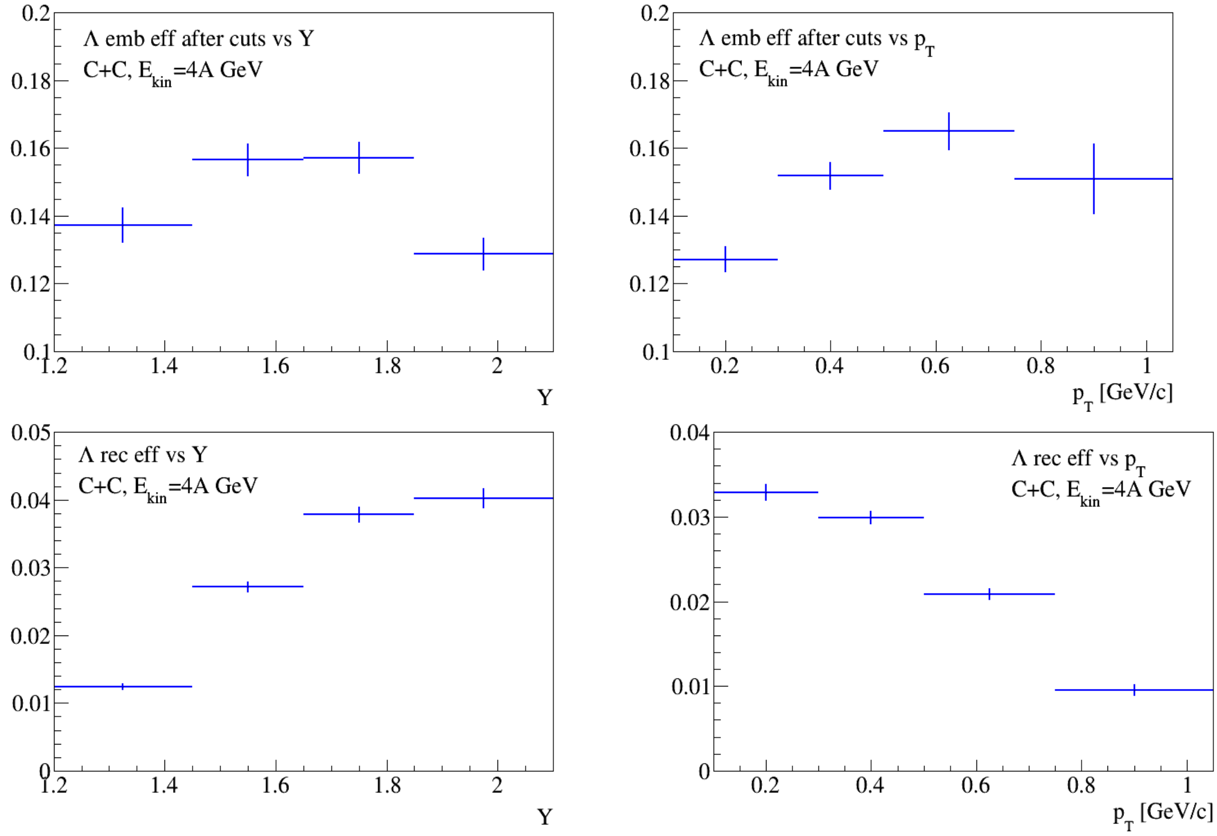

Fig.12a. Λ geometrical acceptance (ε_{acc}); efficiency of reconstruction of embedded Λ after applying kinematic and spatial cuts ($\varepsilon_{emb+cuts}$) and full reconstruction efficiency (ε_{rec}) shown in bins of rapidity y_{lab} in the laboratory frame (left plots) and in bins of p_T (right plots). Results are shown for $C+C$ interactions at 4.0 AGeV carbon beam energy.

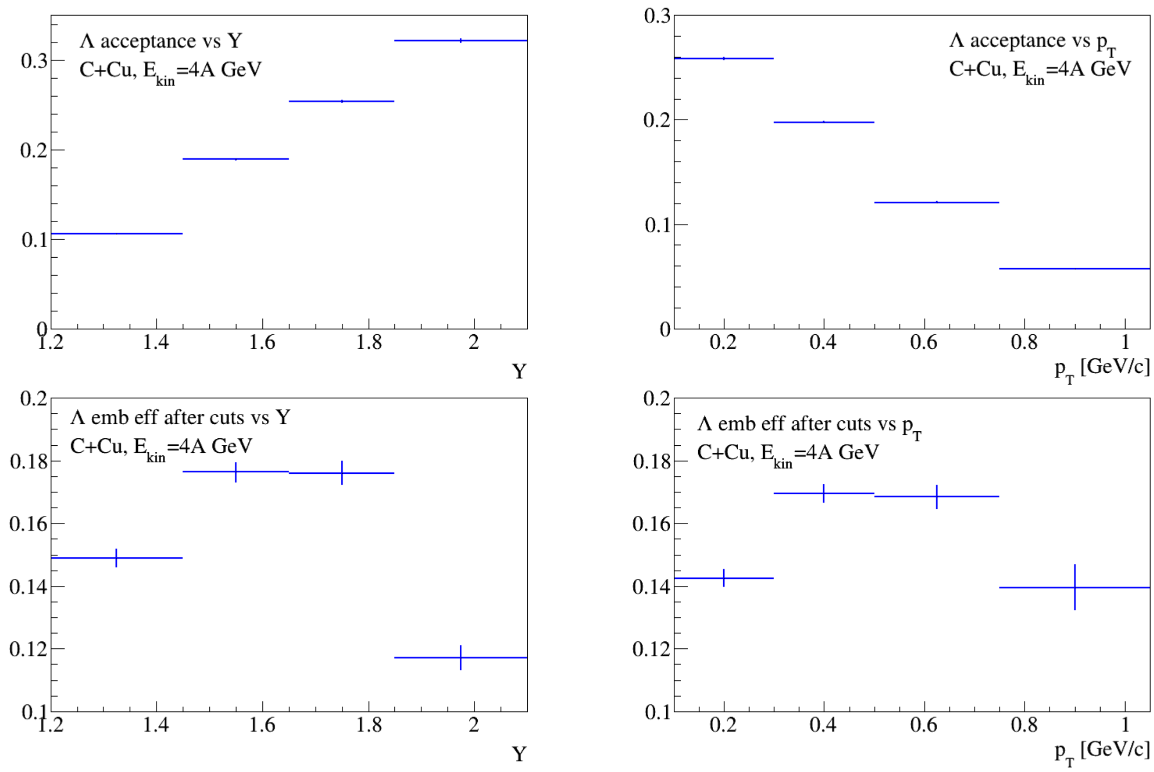

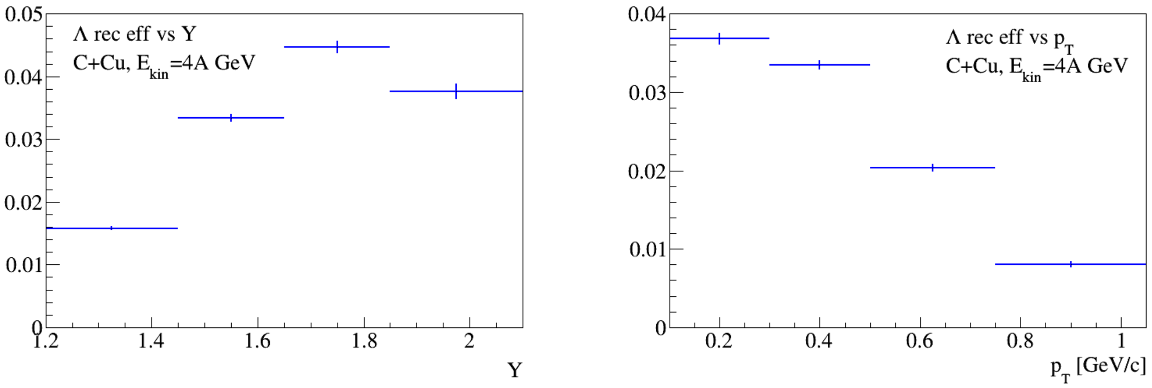

Fig.12b. Λ geometrical acceptance (ε_{acc}), efficiency of reconstruction of embedded Λ after applying kinematic and spatial cuts ($\varepsilon_{emb+cuts}$) and full reconstruction efficiency (ε_{rec}) shown in bins of rapidity y_{lab} in the laboratory frame (left plots) and in bins of p_T (right plots). Results are shown for $C+Cu$ interactions at 4.0 AGeV carbon beam energy.

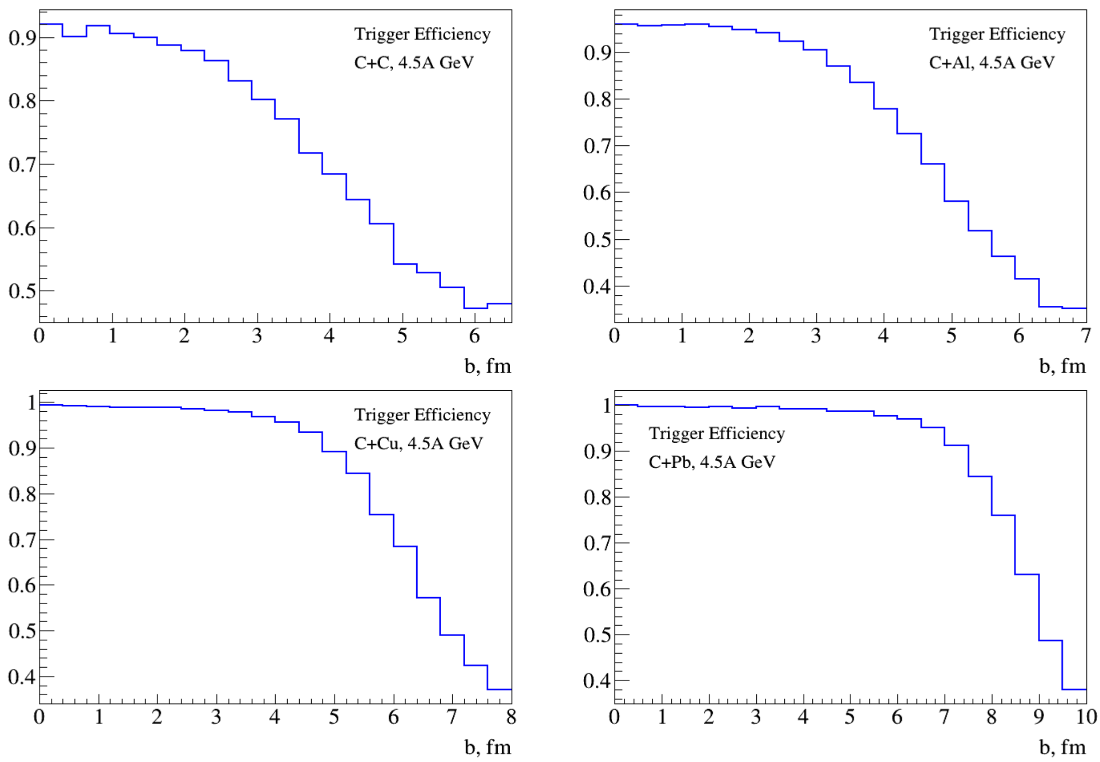

Fig.12c. Trigger efficiency (ε_{trig}) calculated for DCM-QGSM interactions of the carbon beam with the C, Al, Cu, Pb targets shown as a function of the collision impact parameter.

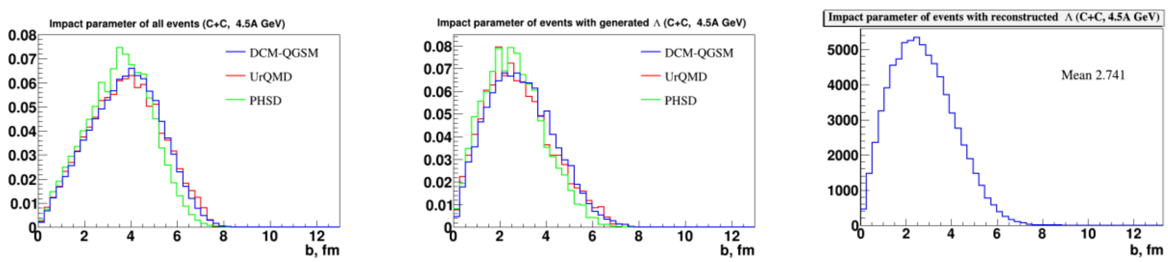

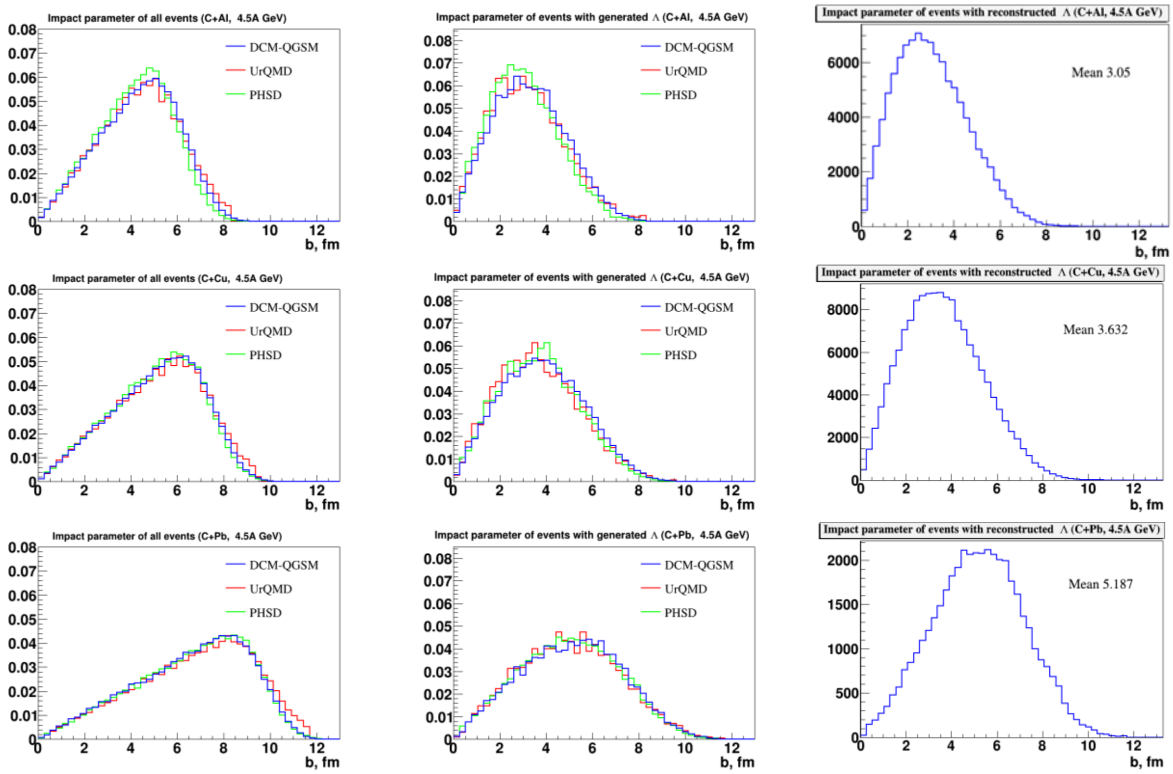

Fig. 12d. Impact parameter distributions of minimum bias interactions of 4.5 AGeV carbon beam with *C*, *Al*, *Cu*, *Pb* targets, generated with the DCM-QGSM, UrQMD and PHSD models (left). Impact parameter distribution of minimum bias events with generated *Λ* hyperons generated with DCM-QGSM, UrQMD and PHSD models (center). Impact parameter distribution of DCM-QGSM minimum bias events with reconstructed *Λ* hyperons (right).

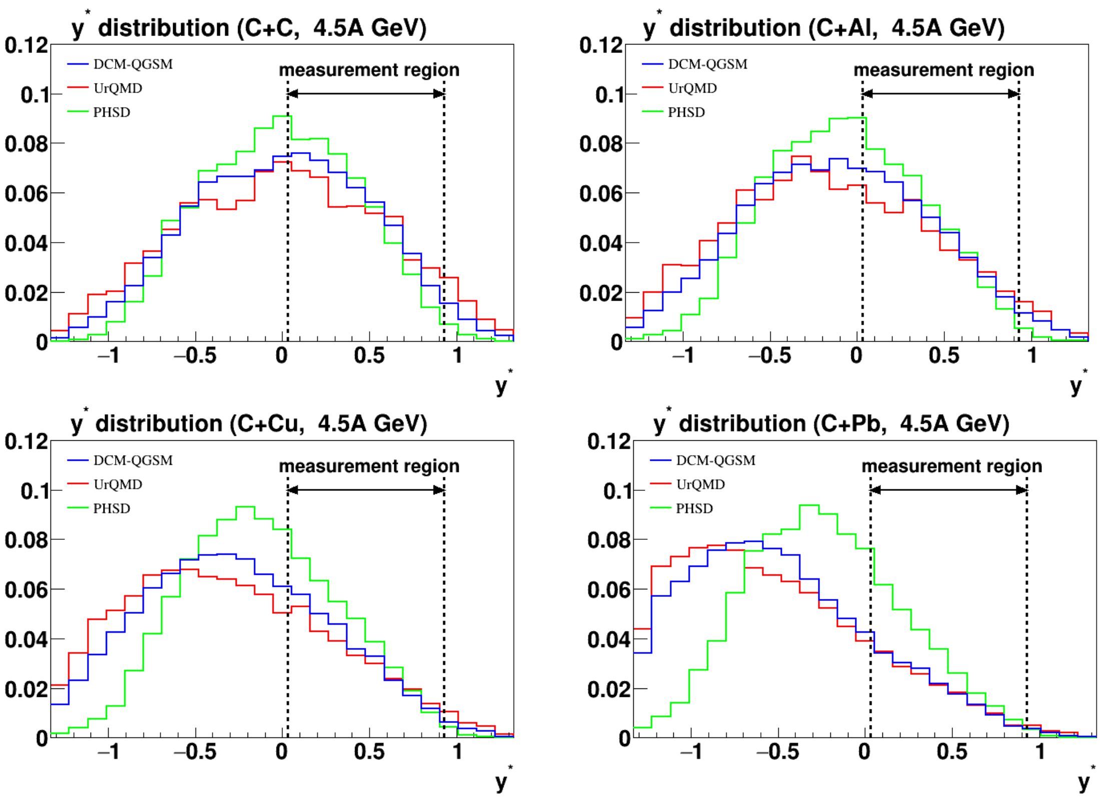

Fig.12e. Rapidity spectra of *Λ* hyperons in minimum bias interactions of 4.5 AGeV carbon beam with *C*, *Al*, *Cu*, *Pb* targets, generated with the DCM-QGSM, UrQMD and PHSD models. The BM@N measurement range in y* is indicated.

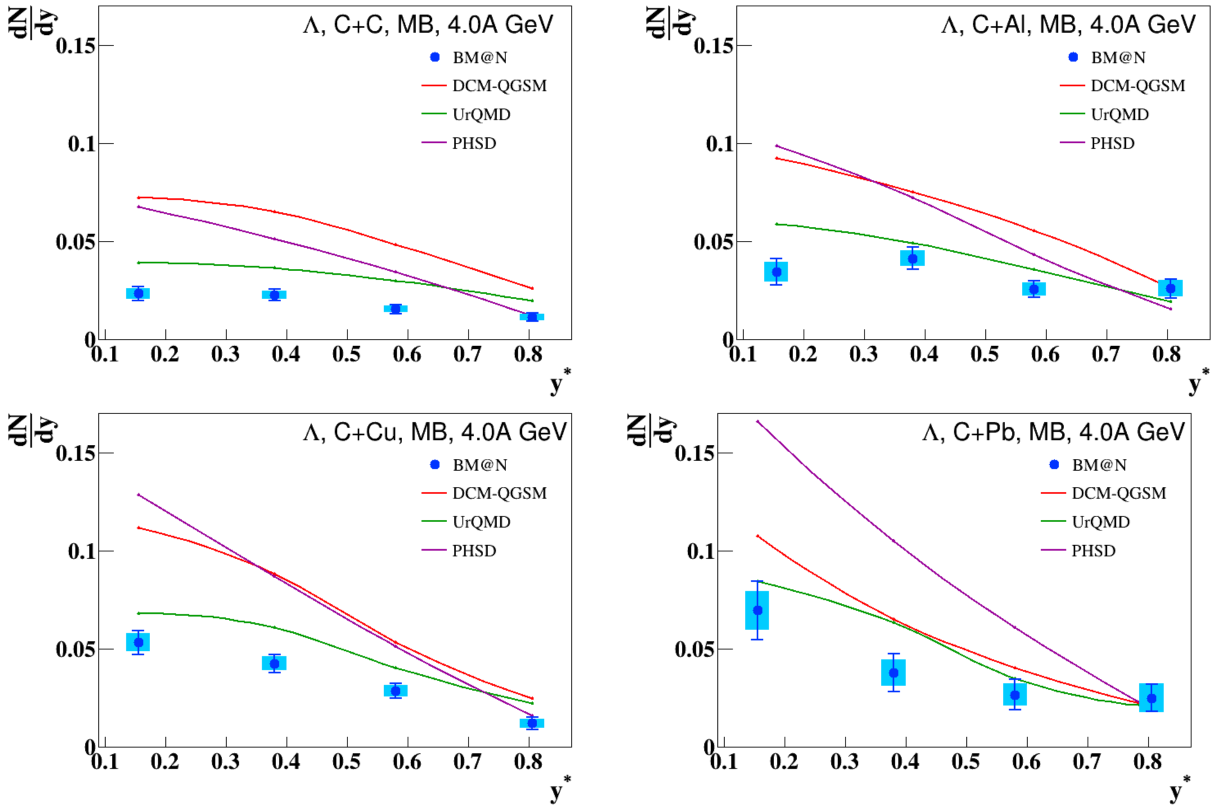

Fig. 13a. Reconstructed rapidity y* spectra of *Λ* hyperons in minimum bias *C+C, C+Al, C+Cu, C+Pb* interactions at 4.0 AGeV carbon beam energy (blue crosses). Predictions of the DCM-QGSM, UrQMD and PHSD models are shown as red, green and magenta lines.

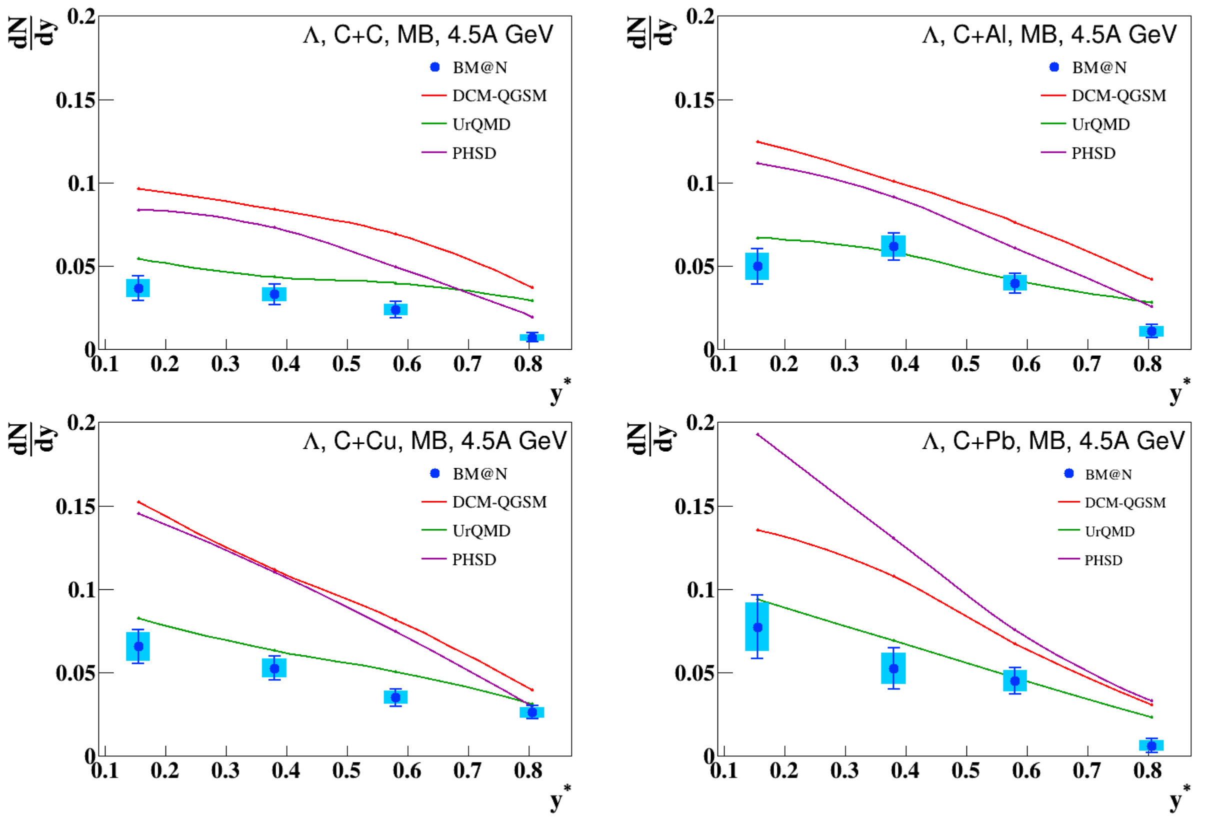

Fig. 13b. Reconstructed rapidity y* spectra of *Λ* hyperons in minimum bias *C+C, C+Al, C+Cu, C+Pb* interactions at 4.5 AGeV carbon beam energy (blue crosses). Predictions of the DCM-QGSM, UrQMD and PHSD models are shown as red, green and magenta lines.

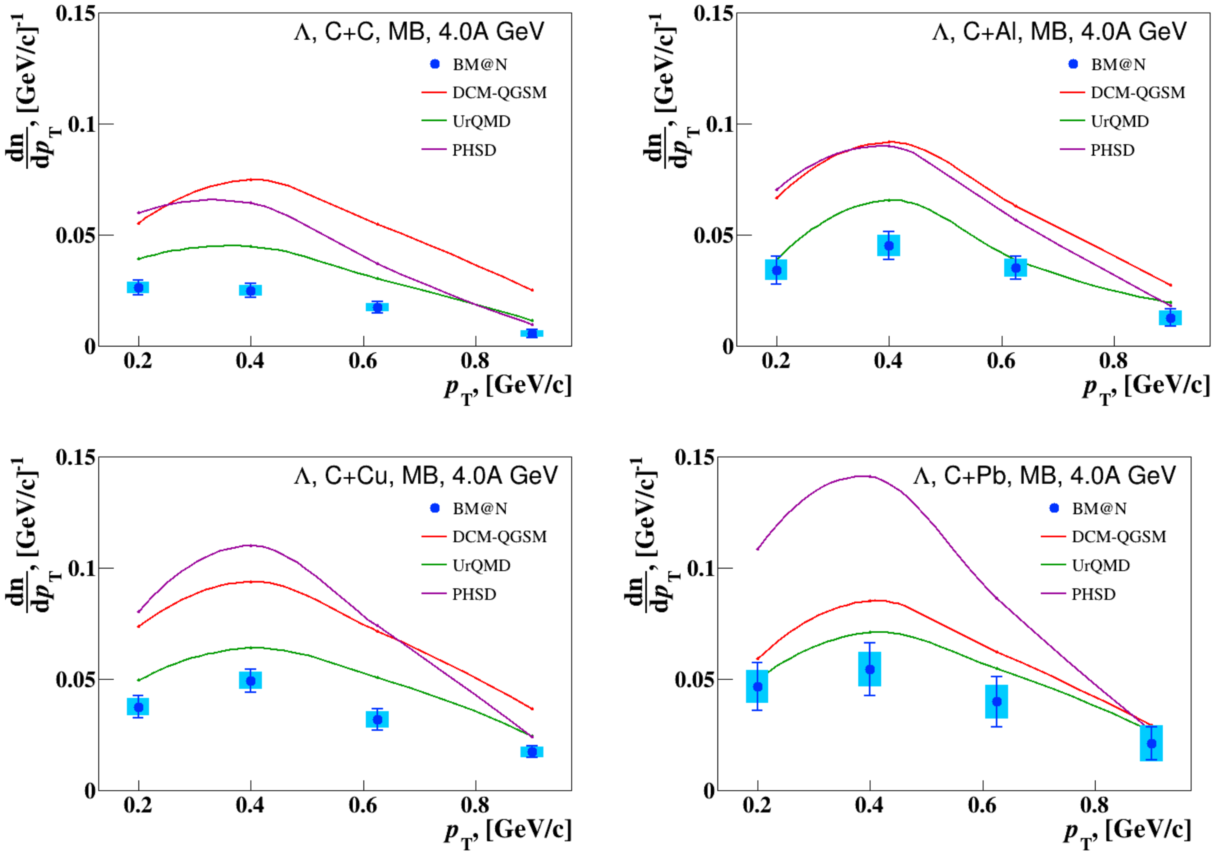

Fig.14a. Reconstructed transverse momentum p_T spectra of Λ hyperons in minimum bias *C+C*, *C+Al*, *C+Cu*, *C+Pb* interactions at 4.0 AGeV carbon beam energy (blue crosses). Predictions of the DCM-QGSM, UrQMD and PHSD models are shown as red, green and magenta lines.

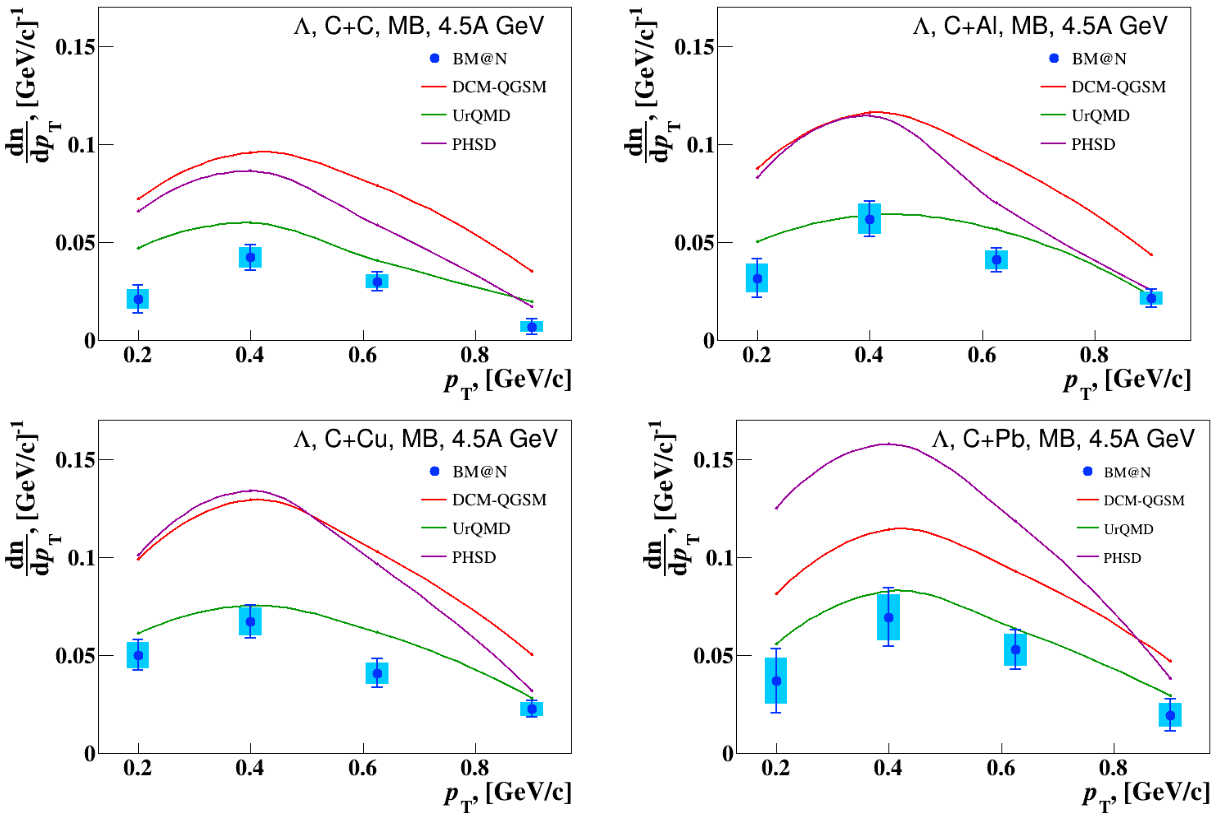

Fig. 14b. Reconstructed transverse momentum p_T spectra of Λ hyperons in minimum bias *C+C*, *C+Al*, *C+Cu*, *C+Pb* interactions at 4.5 AGeV carbon beam energy (blue crosses). Predictions of the DCM-QGSM, UrQMD and PHSD models are shown as red, green and magenta lines.

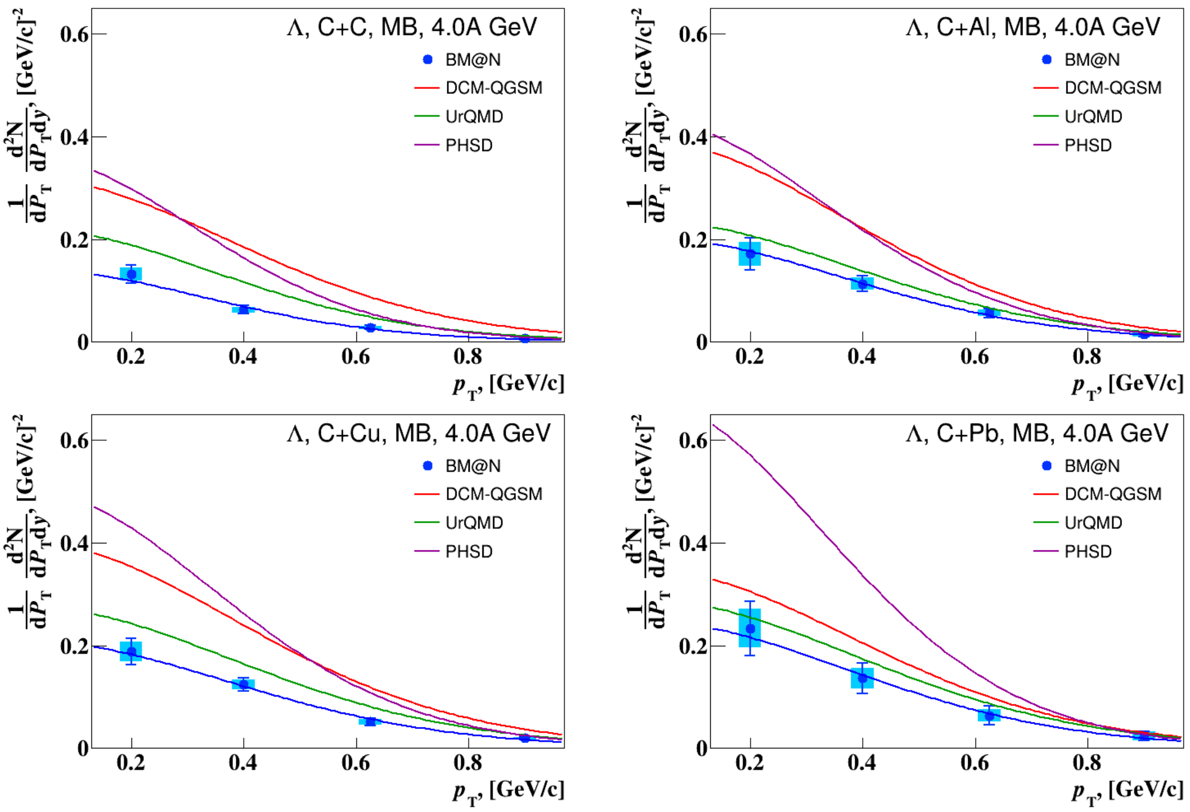

Fig. 15a. Invariant transverse momentum p_T spectra of Λ hyperons in minimum bias *C+C, C+Al, C+Cu, C+Pb* interactions at 4.0 AGeV carbon beam energy (blue crosses). The error bars represent the statistical errors, the blue bands show the systematic errors. Predictions of the DCM-QGSM, UrQMD and PHSD models are shown as red, green and magenta lines.

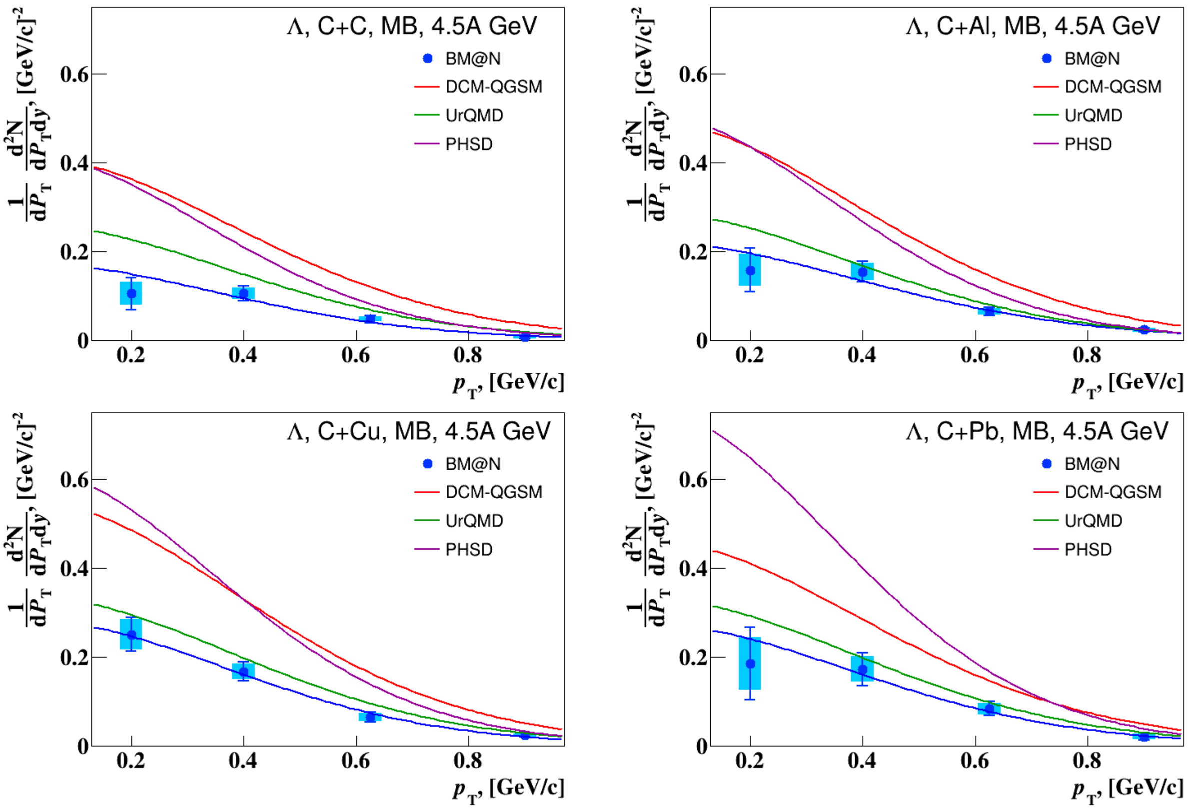

Fig. 15b. Invariant transverse momentum p_T spectra of Λ hyperons produced in minimum bias *C+C, C+Al, C+Cu, C+Pb* interactions at 4.5 AGeV carbon beam energy (blue crosses). The error bars represent the statistical errors, the blue bands show the systematic errors. Predictions of the DCM-QGSM, UrQMD and PHSD models are shown as red, green and magenta lines.

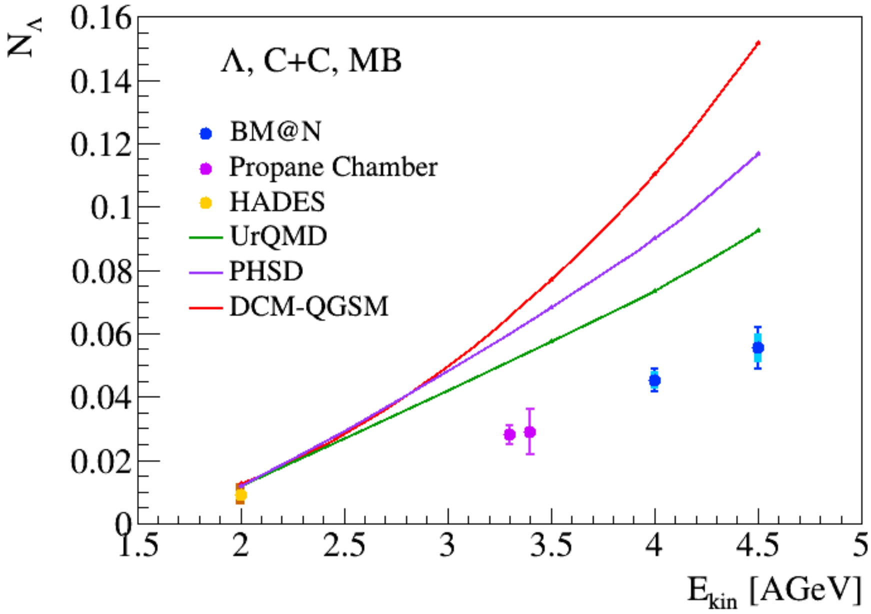

Fig.16a. Energy dependence of Λ yields measured in different experiments. The error bars represent the statistical errors, the blue bands show the systematic errors. BM@N result is compared with data taken from [ArakelianCC], [ArmutCC], [HadesL0]. The predictions of the DCM-QGSM, UrQMD and PHSD models are shown as colored lines.

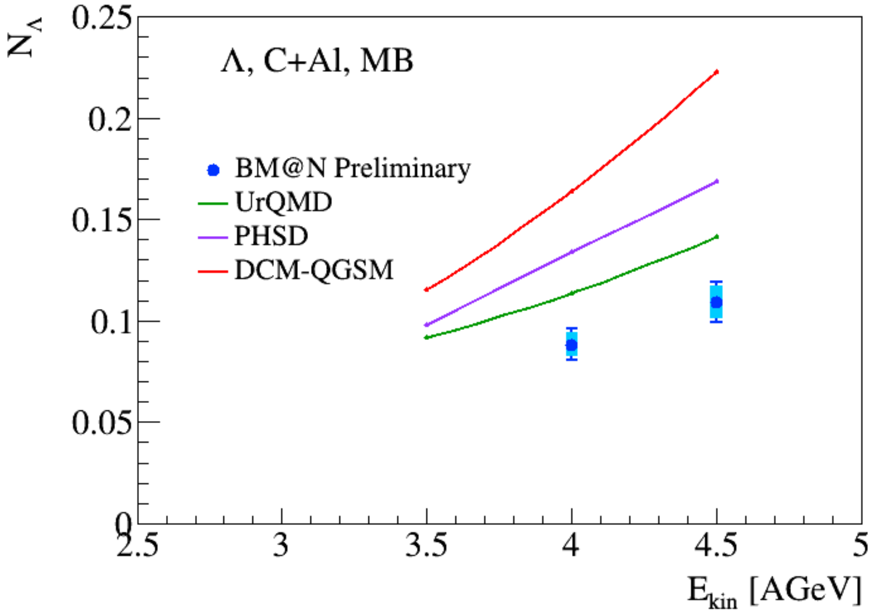

Fig.16b. Energy dependence of Λ yields measured in BM@N *C+Al* minimum bias interactions. The error bars represent the statistical errors, the blue bands show the systematic errors. The predictions of the DCM-QGSM, UrQMD and PHSD models are shown as colored lines.

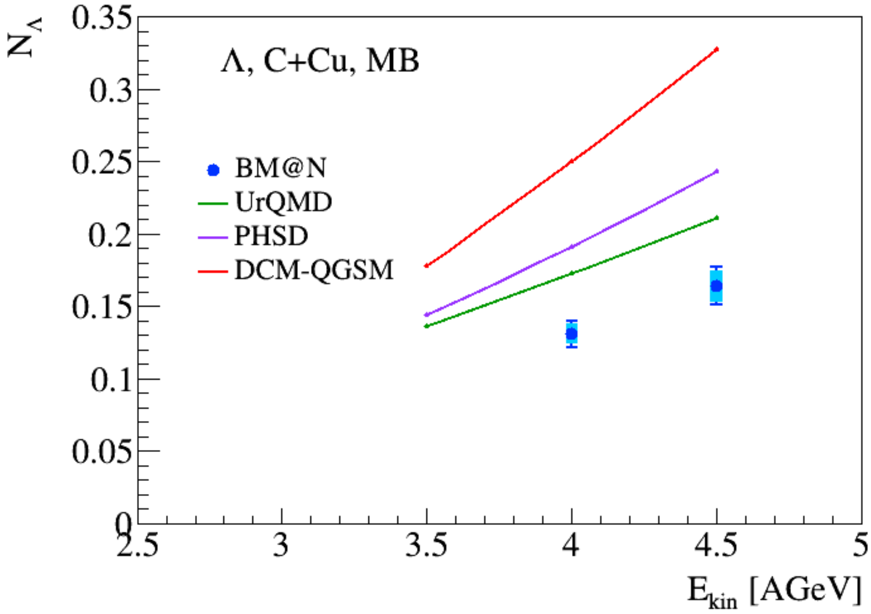

Fig.16c. Energy dependence of *Λ* yields measured in BM@N *C+Cu* minimum bias interactions. The error bars represent the statistical errors, the blue bands show the systematic errors. The predictions of the DCM-QGSM, UrQMD and PHSD models are shown as colored lines.

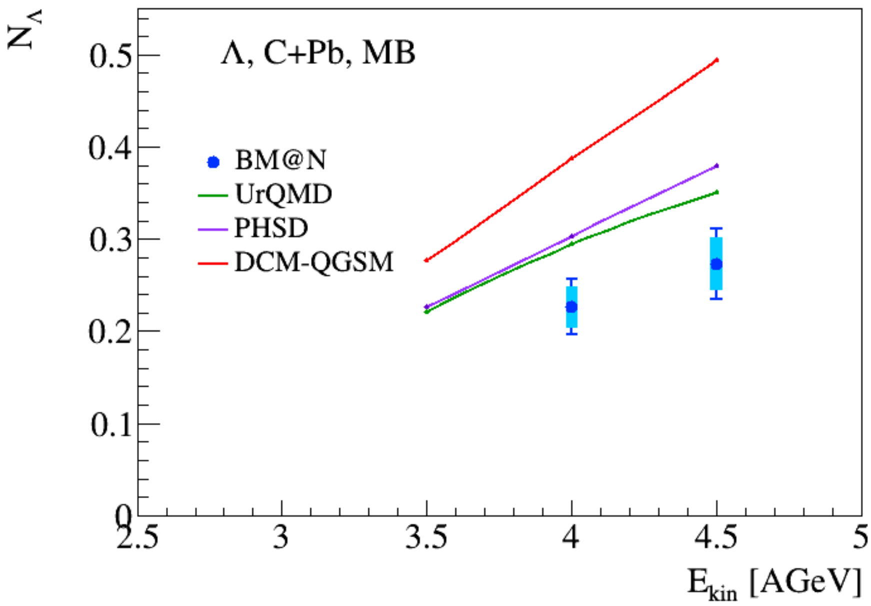

Fig.16d. Energy dependence of *Λ* yields measured in BM@N *C+Pb* minimum bias interactions. The error bars represent the statistical errors, the blue bands show the systematic errors. The predictions of the DCM-QGSM, UrQMD and PHSD models are shown as colored lines.

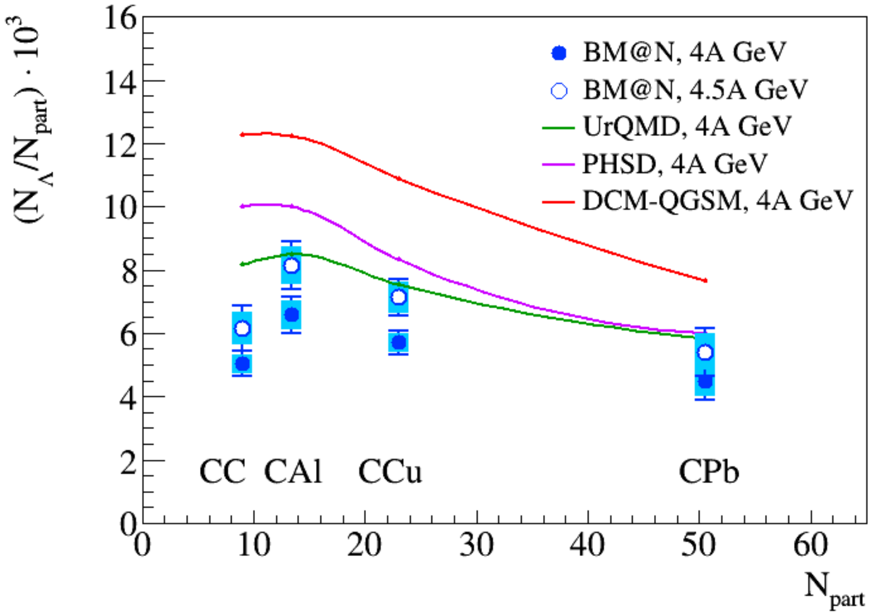

Fig.17. Ratios of the Λ hyperon yields to the number of nucleons-participants measured in BM@N carbon-nucleus interactions at 4.0 and 4.5 AGeV. The error bars represent the statistical errors, the blue bands show the systematic errors. The predictions of the DCM-QGSM, UrQMD and PHSD models are shown as colored lines.

Addendum to Analysis Note 2

Corrections in the data analysis between Preliminary Analysis Note 1 (AN-1) aimed for SQM 2019 and Analysis Note 2 (AN-2)

1)_a mistake is found in the software code for embedding of simulated products of Λ hyperon decay into experimental events. The maximum number of hits in all GEM stations was limited to 200, whereas real numbers of hits were much higher than this limit. As a result the embedding efficiency was artificially lowered. The mistake was corrected in the analysis version for QM2019

2) a correction is made in simulation of Λ decay products embedded into experimental events. Now in simulation the detection efficiencies in all 6 GEM stations are implemented for every experimental run with the probability proportional to statistics of events in the run. The GEM detection efficiencies in different runs are illustrated in Fig.A1. Before that correction in AN-1 average detection efficiencies in GEM stations calculated for the whole set of experimental runs were used. The correction is implemented in the analysis version for QM2019.

3) a correction is made in the calculation of the Λ embedding efficiency. Now the number of reconstructed embedded Λ in every (p_T,y) bin is calculated from the invariant mass spectrum of (p,π^-) after subtraction of combinatorial background under the Λ signal. Before that correction in AN-1 the number of reconstructed embedded Λ was calculated using restricted cuts on differences between parameters of reconstructed and simulated Λ decay products – the same cuts on p_x, p_y, p_z, y were used as for the acceptance calculation (see subsection "Λ reconstruction

efficiency"). This correction is done to avoid usage of MC particle parameters on the level of reconstructed embedded Λ to be consistent with the Λ reconstruction in data. The ratio of the number of reconstructed Λ evaluated in AN-1 to the corrected number of reconstructed Λ is given in Fig.A2 for 16 (p_T,y) intervals and for the whole (p_T,y) range (bin 18 in the plot). The correction was implemented in the analysis version for QM2019.

4) a mistake was introduced during realization of correction 3) in the analysis version for QM2109. To help understand the problem the embedding efficiency and reconstruction efficiency in (p_T,y) intervals are shown in Fig.A3. When filling the numbers of reconstructed embedded Λ in (4x4) intervals of (p_T,y), cuts on p_T<p_{Tmin}, y<y_{min} were missing in the first intervals on p_T and y, while in the highest intervals on p_T and y cuts on p_T<p_{Tmax}, y<y_{max} were missing. As a result, efficiencies calculated in the first and highest intervals on p_T and y were overestimated. The mistake is corrected in the present analysis version after QM2019.

5) a cut on Λ path was adjusted for embedded Λ to get similar reduction of Λ signal as in experimental data. The reduction factor of Λ signal in dependence on the path cut for Λ in data and embedded Λ are shown in Fig.A4. Before that correction in AN-1 a path cut > 2.5 (5) cm was used for Λ in data (embedded Λ) for all the targets. After the adjustment a minimum path for Λ in 4 AGeV data was kept 2.5 cm, while for embedded Λ it was set to 4.5 cm (C), 4.5 cm (Al), 5.0 cm (Cu), 3.5 cm (Pb) to get approximately same reduction factors in the range 0.83-0.85 as in experimental data (see Fig.A4). The correction is implemented in the present analysis version after QM2019.
In Fig.A4a the ratios of normalized rapidity spectra of Λ in 4 AGeV data to normalized rapidity spectra of embedded Λ are fitted by a linear function to illustrate consistency of the experimental and simulated rapidity (energy) spectra of Λ. Deviation of the ratio slope from zero is 0.5σ for C, 2σ for Al, 1.5σ for Cu and 0.5σ for Pb.

6) In AN-1 and analysis version for QM2019 Λ embedding was done using experimental events taken from one selected run per target. In the analysis version after QM2019 Λ embedding is based on experimental events from 3-5 selected runs in different run periods per target to cover different experimental conditions. Herewith, the GEM efficiencies measured in every experimental run of the whole run period were simulated (see Fig.A1 and item 2 of the addendum for more details). The systematic uncertainty was calculated as a r.m.s. of the embedding efficiency evaluated for 4-5 selected experimental runs.

7)_a Data Quality Check was implemented between the analysis version for QM2019 and AN-2: experimental runs were excluded with low fraction of 4-track events (see Fig.A5) and with hardware problems in GEM detectors caused by HV trips or failures in readout electronics (see Fig.A6). Different fractions of the run time with HV trips and hardware problems resulted in the spread of the efficiencies for different runs. The data quality run selection is implemented in the present analysis version after QM2019.

8) After QM2019 the barrel trigger detector efficiency was recalculated using the full set of simulated events for all the data samples (C,Al,Cu,Pb). The recalculated barrel detector efficiencies are somewhat smaller than those used in AN-1 and QM2019 versions of the

analysis: by a factor 1.11 for C+C, 1.06 for C+Al and 1.03 for C+Cu. The cross sections and yields given in AN-2 take into account the recalculated barrel detector efficiency. Later the difference in the AN-1 and AN-2 barrel detector efficiencies was traced to different simulated positions of the C,Al,Cu targets. In the AN-2 version target positions were simulated from reconstructed experimental vertex distributions in (x,y,z). It is found to be not right because the target positions in the barrel detector were fixed in (x,y,z) and not spread due to the experimental resolution. The trigger barrel detector efficiency should be taken from AN-1. Trigger efficiency calculated for QGSM events with reconstructed Λ hyperons shown in Fig.A7 as a function of impact parameter for the C,Al,Cu,Pb targets. Trigger efficiency calculated for all generated QGSM events shown in Fig.A8 for the same targets. As a result cross sections and yield in AN-2 should be reduced by factors 1.11 for C+C, 1.06 for C+Al, 1.03 for C+Cu. The measured Λ hyperon yields presented in the QM2019 poster and given in AN-2 (using the AN-1 version of the trigger efficiency) are presented in the table:

4 AGeV	***Λ yield QM2019***	***Λ yield AN-2 (trigger efficiency from AN-1)***	***Difference / systematic error***
C+C	0.0129±0.0011±0.012	0.0147±0.0011±0.009	+0.0018 (+1.5 σ)
C+Al	0.0241±0.0020±0.019	0.0270±0.0023±0.018	+0.0029 (+1.5 σ)
C+Cu	0.0333±0.0026±0.024	0.0297±0.0020±0.015	-0.0036 (-1.5 σ)

The difference in Λ yields (and cross sections) between QM2019 and AN-2 (trigger efficiency from AN-1) is +/- 1.5 of the systematic uncertainty given in the QM2019 poster. The differences are resulted from mistake 4) corrections 5) , 6) and a run quality check 7).

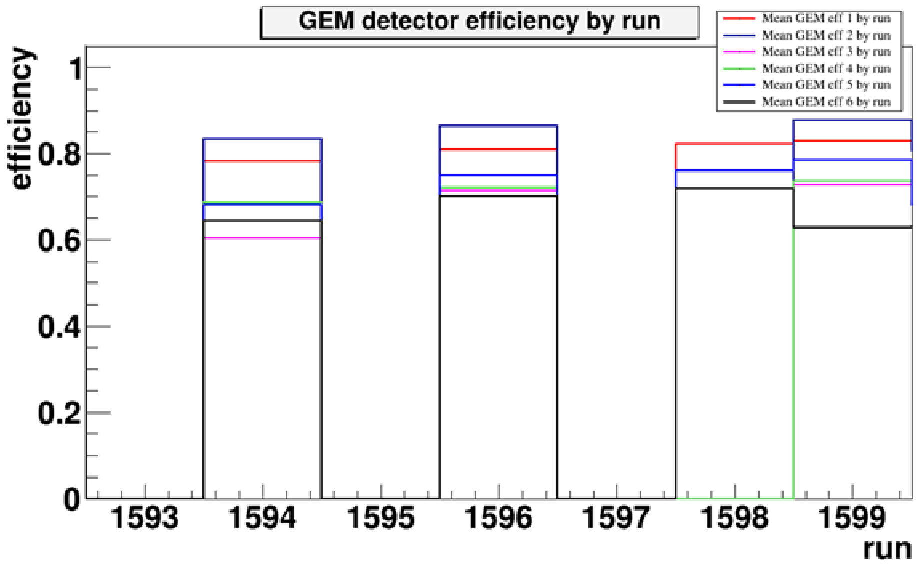

Fig.A1. GEM detection efficiencies for different experimental runs. Efficiencies for 6 GEM stations are shown with different colors.

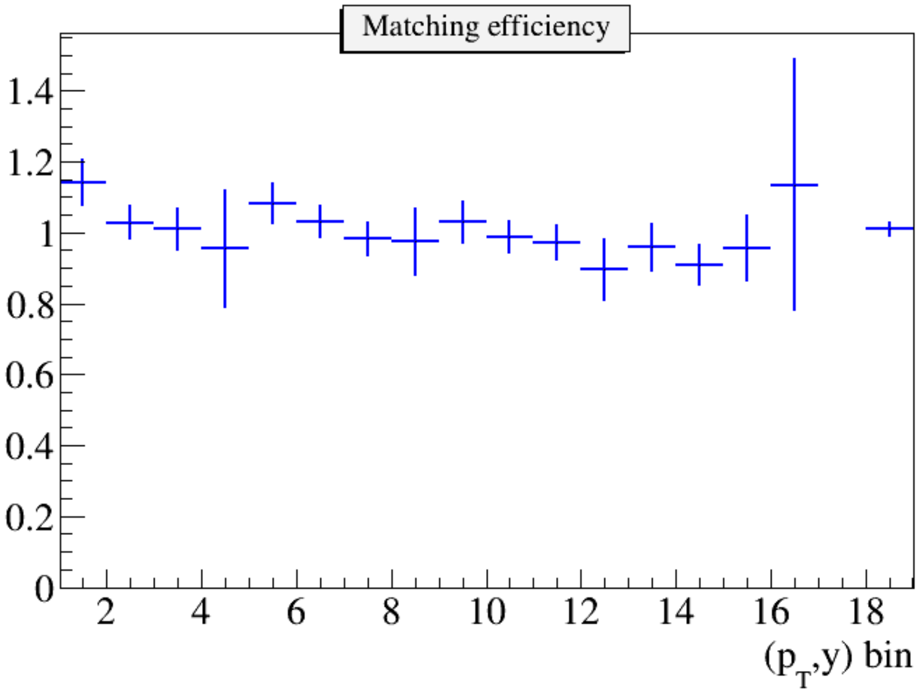

Fig.A2. Ratio of the number of reconstructed Λ evaluated in AN-1 to the corrected number of reconstructed Λ evaluated from the *(p,π-)* invariant mass spectra (analysis version for QM2019). The ratio is given for 16 (p_T,y) intervals and for the whole (p_T,y) range (bin 18).

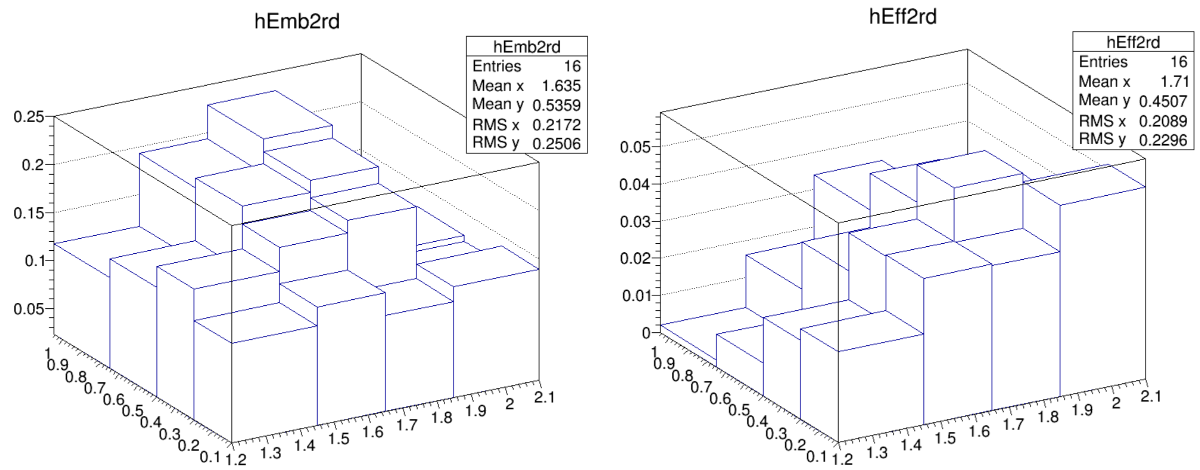

Fig.A3. Embedding efficiency (left plot), full reconstruction efficiency (right plot) for (4x4) intervals in (p_T,y): $0.1<p_T<1.05$ GeV/c, $1.2<y<2.1$.

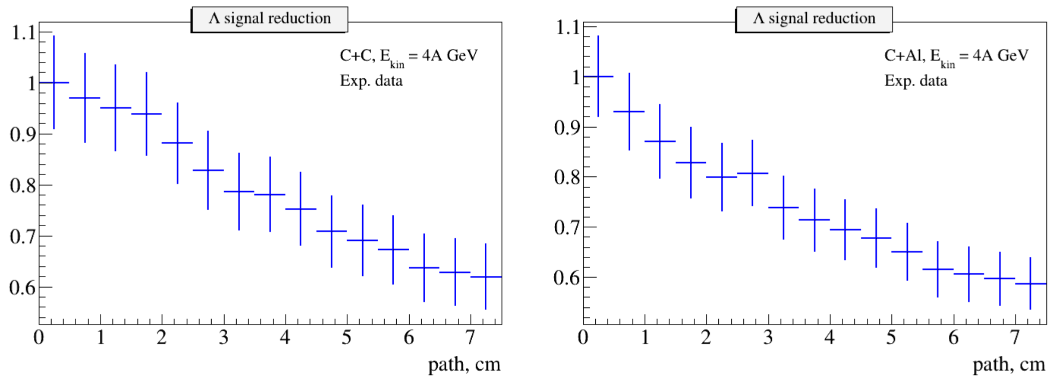

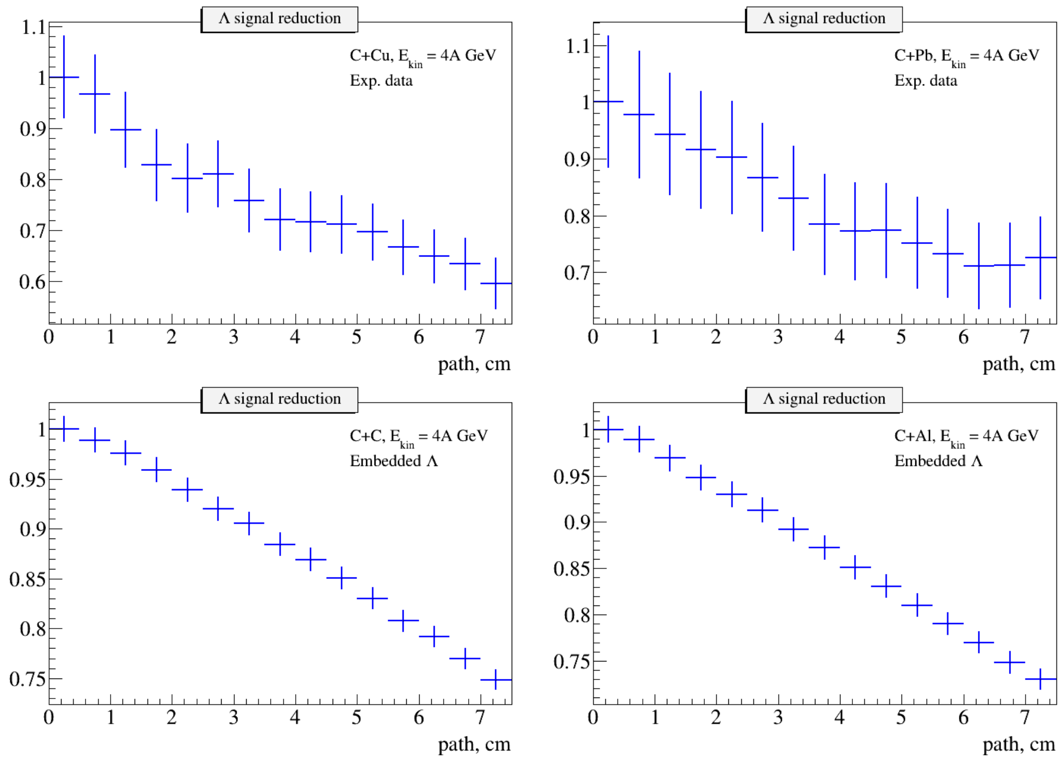

Fig.A4. Reduction factor of Λ signal in dependence on the path cut (cm) for Λ in data: upper plots for C+C,C+Al, middle plots for C+Cu,C+Pb, lower plots for embedded Λ (C+C, C+Al).

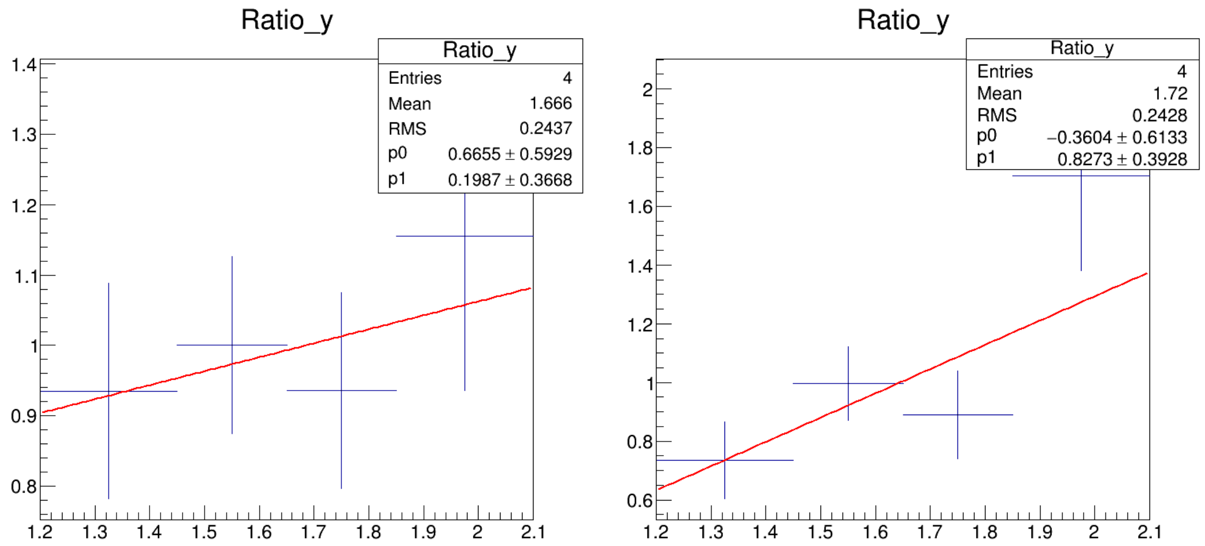

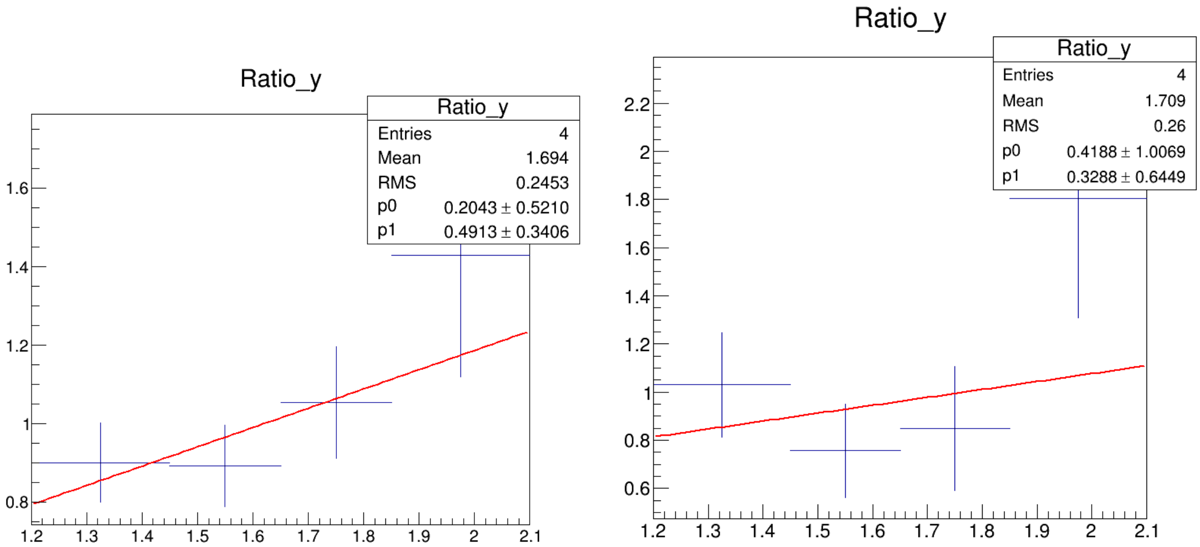

Fig.A4a. Ratio of normalized Λ data rapidity spectrum to normalized rapidity spectrum of embedded Λ. Ratios for C,Al data are presented in the upper plots, ratios for Cu,Pb data are presented in the lower plots.

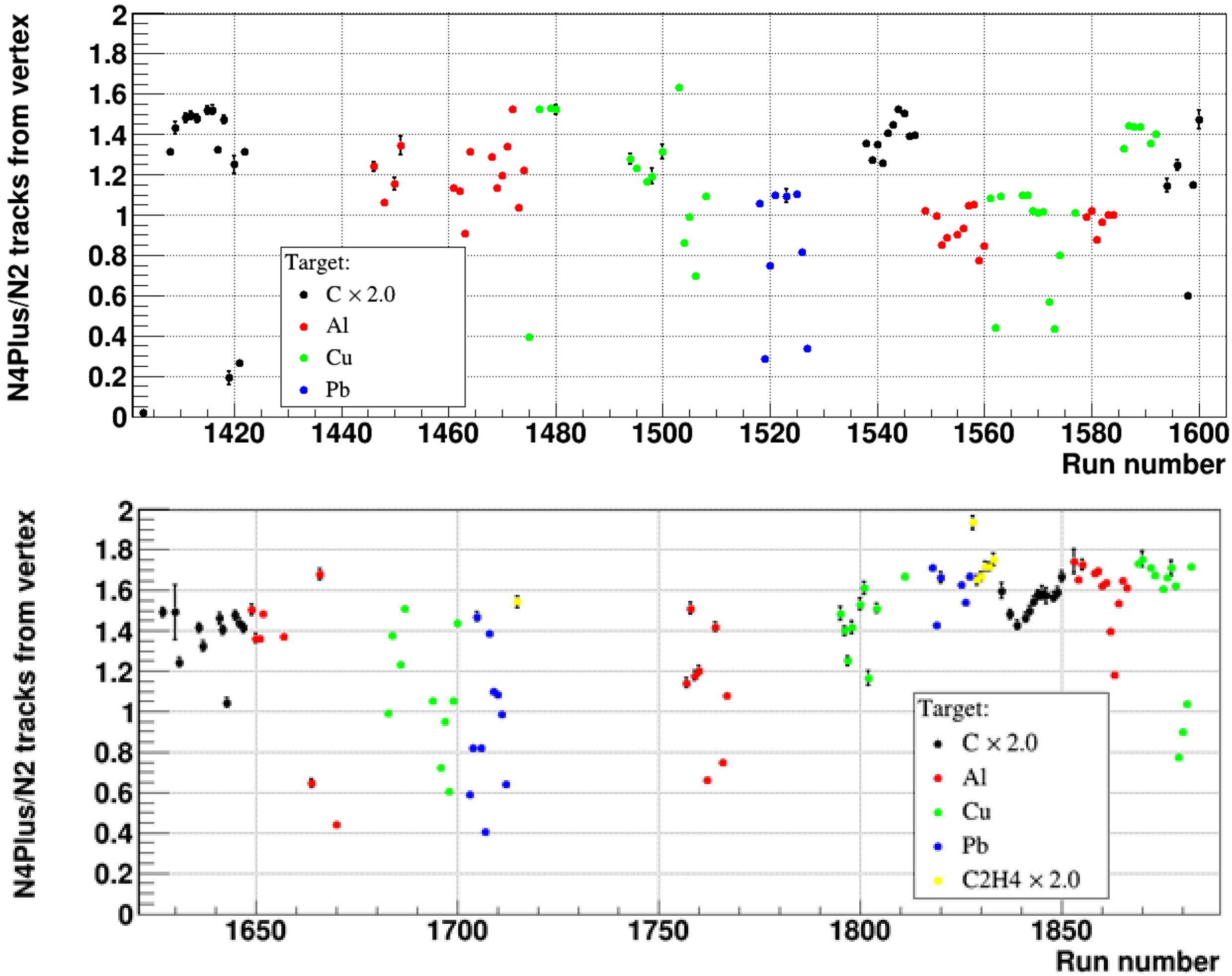

Fig.A5. Ratio of the number of events with 4 and more reconstructed tracks (assuming topology with ≥2 tracks from the vertex and two tracks from Λ decay) to the number of events with only 2 reconstructed tracks from the vertex vs the run number. Runs with the ratio < 0.7 were excluded for the data analysis. The upper plot is for 4 AGeV data, the lower plot is for 4.5 AGeV data.

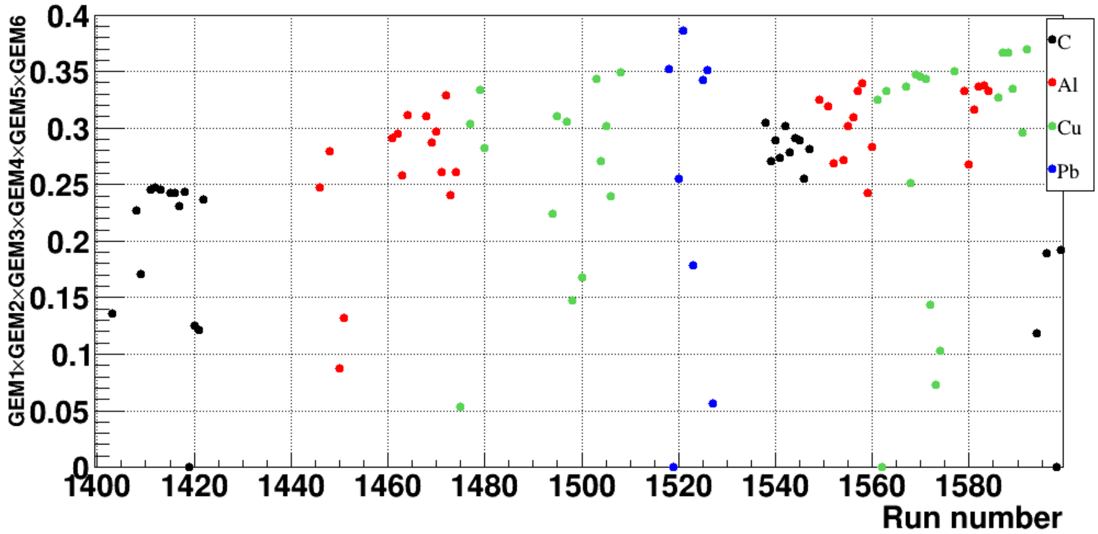

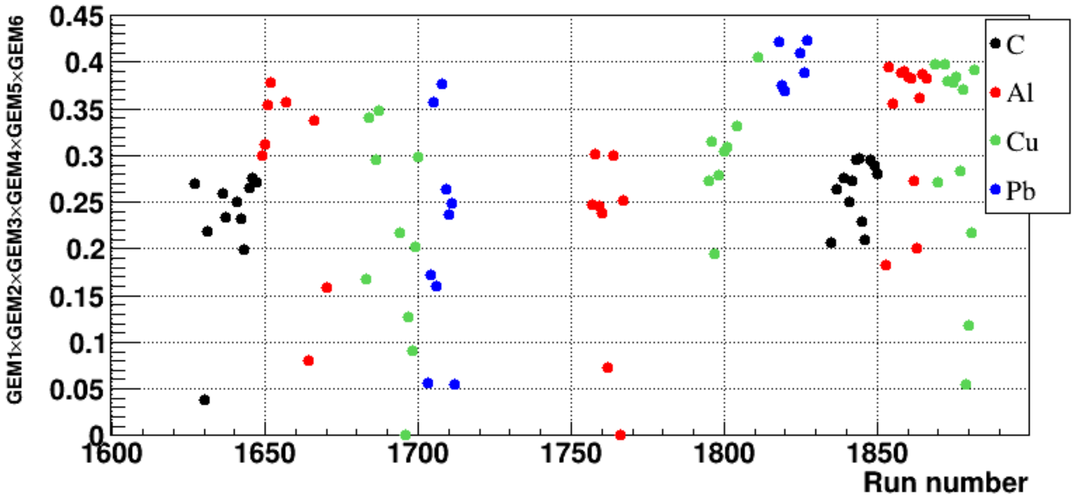

Fig.A6. Product of the track detection efficiencies in 6 GEM stations vs the run number. Runs with the efficiency product < 0.18 were excluded for the data analysis. The upper plot is for 4 AGeV data, the lower plot is for 4.5 AGeV data. The spread of the efficiencies in runs is caused by HV trips during a run or by hardware problems with readout electronics.

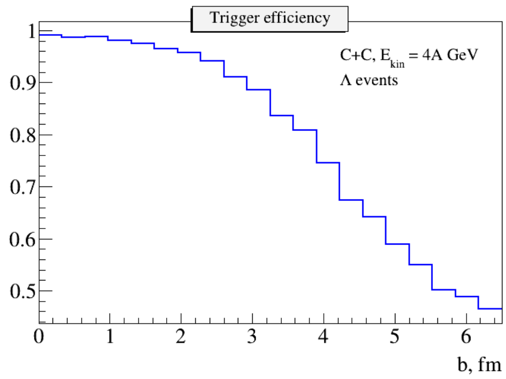

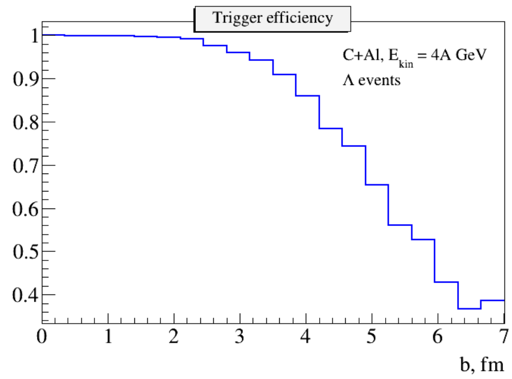

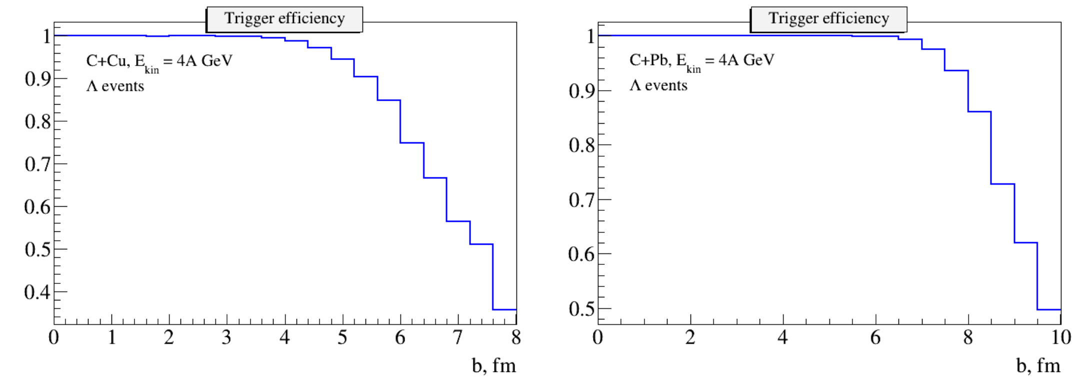

Fig.A7. Reduction factor of Λ signal in dependence on the path cut (cm) for Λ in data: upper plots for C+C,C+Al, middle plots for C+Cu,C+Pb, lower plots for embedded Λ (C+C, C+Al).

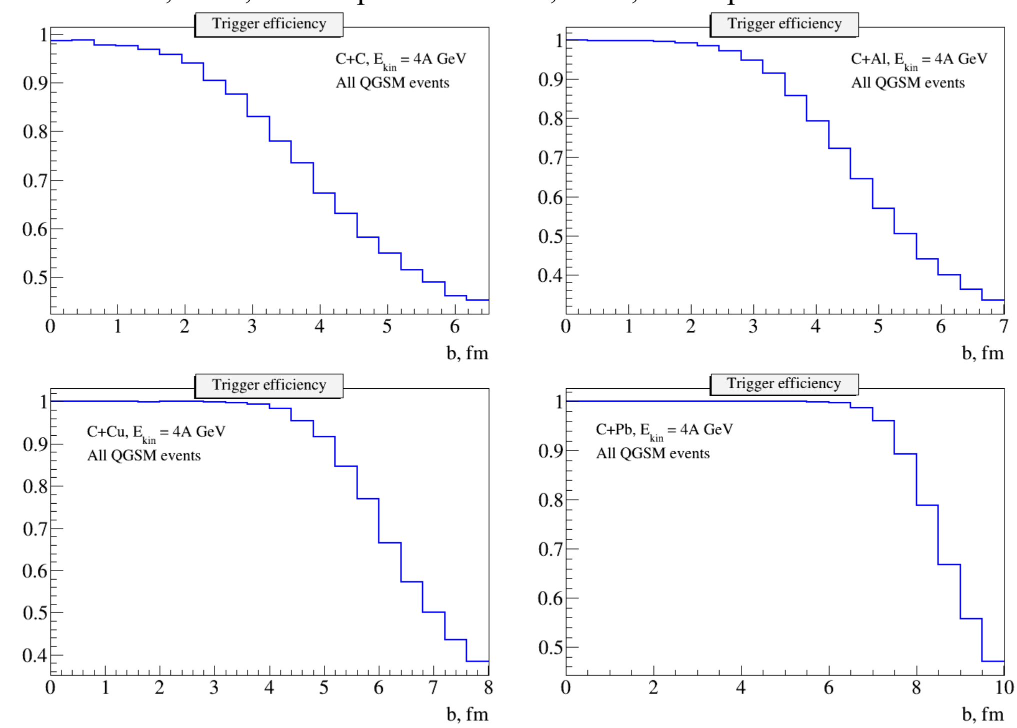

Fig.A8. Reduction factor of Λ signal in dependence on the path cut (cm) for Λ in data: upper plots for C+C,C+Al, middle plots for C+Cu,C+Pb, lower plots for embedded Λ (C+C, C+Al).

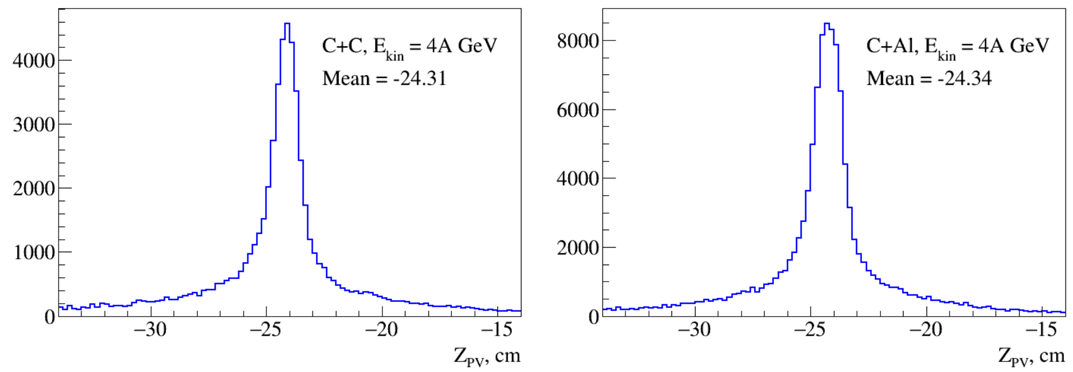

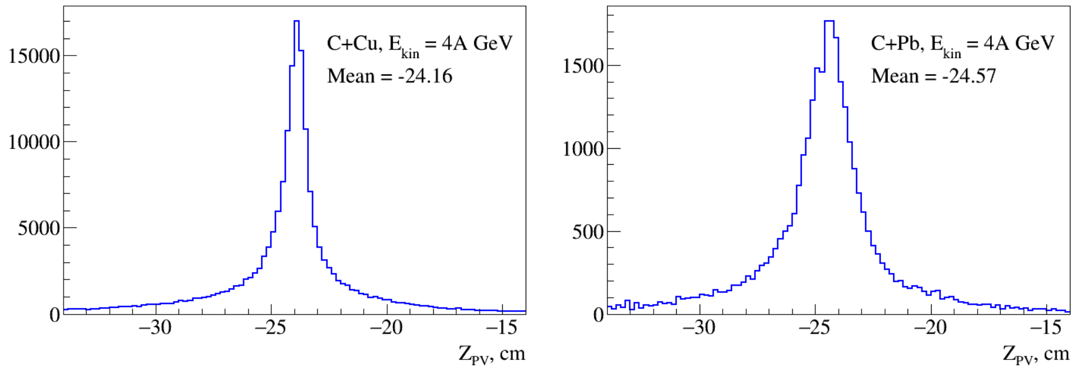

Fig.A9. Z_{PV} primary vertex distribution in 4 AGeV C+C,Al,Cu,Pb data. The analysis cut $|Z_{PV}-Z_{mean}|<10$ cm is not applied in these plots.

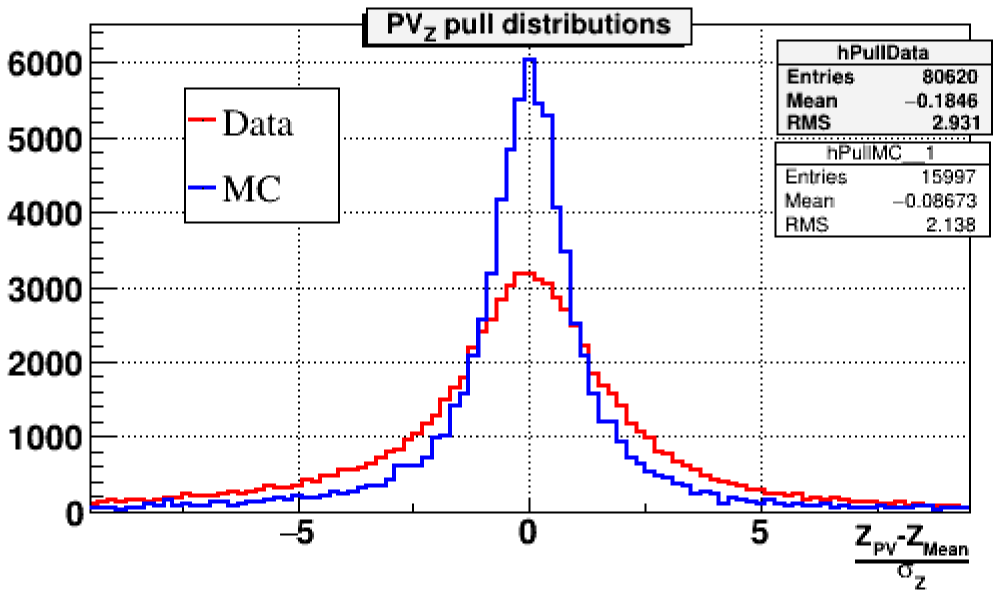

Fig.A9a. Pull distributions for reconstructed primary vertex Z_{PV} in 4 AGeV C+Cu data and simulation.